Presence-only approach to assess landslide triggering-thickness susceptibility: a test for the Mili catchment (north-eastern Sicily, Italy)

Title: Presence-only approach to assess landslide triggering-thickness susceptibility. A test for the Mili catchment (North-Eastern Sicily, Italy).

Authors: Lombardo L.[1,2] Fubelli G.[3] Amato G.[4] Bonasera M.[4]

Division of Physical Sciences and Engineering. King Abdullah University of Science and Technology. Tuwal 23955-6900, Kingdom of Saudi Arabia.

Department of Geosciences, University of Tübingen. Rümelinstraße 19-23, 72070 Tübingen, Germany.

Department of Earth Sciences, University of Torino. Via Valperga Caluso 35, 10125 Torino, Italy.

Department of Sciences, Roma Tre University. Largo S.L. Murialdo 1, 00146 Roma, Italy

Corresponding author: Luigi Lombardo, Department of Earth and Sea Sciences, Via Archirafi, 20 - 90123 Palermo - Tel.: +39 091 23864649; fax: +39 091 6169908, University of Palermo, Italy.

Email: luigi.lombardo83@gmail.com

Abstract

This study evaluates the performances of the presence only approach, Maximum Entropy, in assessing landslide triggering-thickness susceptibility within the Mili catchment (Sicily, Italy). This catchment underwent several meteorological stresses, resulting in hundreds of shallow rapid mass movements between 2007 and 2011. In particular, the area has become known for two disasters, which occurred in 2009 and 2010; the first weather system did not pass directly over the catchment however peak rainfall was registered over the basin during the second meteorological event. Field data were collected to associate the depth from the slope surface that material was mobilised at the triggering zone to each mass movement within the catchment. This information has been used to model the landslide susceptibility for two classes of processes, divided into shallow failures for maximum depths of 1m and deep ones in case of values equal or greater than 1m. Topographic attributes from a 2m DEM were used as predictors, together with medium resolution vegetation indexes derived from ASTER scenes and geological, land use and tectonic maps. The presence-only approach discriminated between the two depth classes at the landslide trigger zone, producing excellent prediction skills associated with relatively low variances across a set of 50 randomly generated replicates. The role of each predictor was assessed to ascertain the significance to the final model output. This work uses simple field measurements to produce triggering-thickness susceptibility, which is a novel approach and may perform better as a proxy for landslide hazard assessments with respect to more common susceptibility practises.

Keywords:

Landslide triggering-thickness susceptibility, Maxent, Presence-only, rainfall-induced shallow mass movements.

1. Introduction

Since the birth of the landslide susceptibility concept (Brabb 1983), the main progress for catchment scale research has focused on statistical methods. In particular, a broad variety of applications have applied presence-absence (Iovine et al. 2014) approaches to calculate the probability of occurrences of different landslide phenomena and trigger mechanisms (Capitani et al. 2013; Harders et al. 2011; Lombardo et al. 2014). Recent developments in statistics have enabled new Geographical Information Systems (GIS) approaches combined to presence-only methods (Bradley 2015), to investigate the spatial relationship between the presence of a given environmental process and a set of covariates (Moosavi and Niazi, 2015). Ecologists have adopted this approach extensively (e.g., Procter et al. 2015; West et al. 2015) with over 1000 published applications since 2006 (Merow et al. 2013), while the geomorphological community have only recently started to assess the applicability of presence-only methods, using the Maximum Entropy (Convertino et al. 2013; Davis and Blesius 2015; Dickson and Perry 2015) algorithm developed at Princeton University. Maximum Entropy does not rely on the negatives (no-landslides or stable conditions) to derive spatial predictive functions and as a consequence, the landslide mapping as well as the adopted predictors need to be accurate to produce good results. To satisfy this requirement, the authors carried out a detailed geomorphological study aimed at directly mapping the landslide scenario in the small catchment of Mili (Messina, Italy) and specifically differentiating the depth to which materials were

mobilised at the crown of each mass movement. Within the Mili catchment, widespread rainfall-triggered landslides have occurred on several occasions between 2007 and 2011, sometimes triggered by peak storm rainfall (March 2010 and 2011) or by storms that did not affect the entire catchment (October 2007 and 2009). We modelled the cumulated landslide distribution in Mili catchment between 2007 and 2011, adopting the Maximum Entropy method and a set of DEM-derived, remotely-sensed and thematic predictors, to assess the landslide triggering-thickness susceptibility. Fifty models were generated to assess the uncertainty of the prediction (Cama et al. 2015; Petschko et al. 2014).

2. Materials

2.1 Study area

The study area is located in the North-eastern-most sector of Sicily (Italy) with an approximate areal extent of 10 km^2 (Fig. 1a). The catchment of the Mili stream is located to the East of the Peloritani Belt (De Guidi and Scudero 2013), an area characterised by deeply incised V-valleys filled with alluvial deposits. Elevations within the catchment peak at approximately 1060m a.s.l.; slopes are steep, ascending from sea level to peak elevations in a relative short length of 5.6km. Mili is situated within the Calabrian-Peloritan Arc (Aldega et al. 2011; Comerci et al. 2015), which is a south-verging thrust resulting in a strong segmentation of the whole system. The aforementioned tectonic effect, its torsion and the south eastward migration are linked to the Tyrrhenian Sea opening. This event dictates local geology, with respect to the anti-clockwise rotation of the Italian peninsula and the Ionian plate subduction under the arc (15 My ago; Carafa et al. 2015). The complex tectonic setting is responsible for the geological stack of different Alpine tectonic units within the southern sector of the Calabrian-Peloritan Arc (Fig. 1a), which locally includes a crystalline basement underlying remnants of Meso-Cenozoic covers (Massari and Prosser 2013). The lithologies belonging to the basement consist of: i) phyllites of the Mandanici Unit; ii) Dolomites and Limestones of the Alì Unit; iii) phyllites of the Piraino Unit; iv) gneiss and paragneiss of the Aspromonte Unit; v) Mela Unit. The latter extensively outcrops in the study area consisting of medium to high metamorphic rocks: paragneiss, micaschists and amphibolites (Trigila et al. 2015). Synorogenic terrigenous deposits at the top of the metamorphic units are stacked in overlapping successions, these being delimited by angular nonconformities. The portion of the catchment closest to the coastline contains more recent deposits, which outcrop as conglomerates and marl clays (Miocene), sand and gravel (Pleistocene) and recent Holocene deposits (Giunta et al. 2012). Figure 1b summarises the outcropping lithologies (Lentini et al., 2007) that are found within the Mili catchment. Field examples of these lithologies are shown in figure 2.

2.2 Landslide recognition

The landslides considered in the present work represent events between 2007 and 2011. During this time, significant rainfall events occurred up to a week before landsliding, involving approximately 250mm (2007), 300mm (2009), 150mm (2010), and 250mm of rainfall (2011) (Fig.3). These values were recorded by the rain gauge at St. Stefano Briga station, located approximately 3 km to the south of the study area. The landslide detection was performed by a two-step method. The first step focussed on mapping the scarps over the slopes, using orthophotos provided by the Territory and Environment Department of the Sicilian government (ARTA 2008 – Assessorato Regionale Territorio e Ambiente) and the National Civil Protection (PCN 2009, Protezione Civile Nazionale), together with Google Earth imagery (2006, 2010, 2011, 2012). Each landform was digitised as a polygon within a GIS environment. This cartographic base was referenced during a geomorphological campaign carried out between September and November 2014. The fieldwork produced a 1:5000 survey within the Mili catchment. One hundred and fifty landslides were identified and grouped into four main typologies. Falls, rotational slide, debris slides, debris flows accounted for 6, 7, 12, 125 mass movements, respectively (e.g. Fig.4). Analysis in this paper excludes the falls and rotational slide classes, in order to focus on landslides caused by the same triggering mechanism. Debris flows and debris slides were combined to represent the superficial landsliding processes occurring within the catchment. During the fieldwork, information for each landslide were retrieved and validated, with respect to the available literature. The following observations and measurements were collected for each landslide: a GPS position of the apex, outcropping lithology, crown slope angle, presence of proximal tectonic alignments, and the cover thickness immediately above the landslide apex. The thickness parameter is shown in Fig.5a for the full landslide sample in the study area, and the geographic distribution of the reclassified thicknesses is shown in Figure 5b. The latter shows two classes: landslides with an initial thickness less than a metre (hereafter *thin*), and landslides with an initial thickness equal or greater than one metre (hereafter *thick*).

3. Material and methods

3.1 Predictors

The dataset adopted for the modelling consisted of ten covariates, five of which were obtained from a 2m cell resolution HRDEM. The source LIDAR survey (ARTA 2008; Cama et al. 2015) was carried out prior to the oldest mass movement identified within the catchment and it was used to represent predisposing conditions at a small scale. Two vegetation-related predictors (15m cell resolution) were calculated from the ASTER scene acquired on (10/07/2009), and to express landslide conditions pertaining to a wider neighbourhood. Geological thematic information (Lentini et al., 2007) have been included: (i) outcropping lithology (hereafter "Geology"), and (ii) distance from faults (hereafter "Tectonic"). Land use (Corine 2006, hereafter "Use") was also included, this being validated during fieldwork activities. These predictors were selected to take into account influences on landslide triggering, typical of catchment-scale processes. The full list of covariates included: i) Aspect (Zevenbergen and Thorne 1987), ii) Burn Index (Hudak et al. 2004), iii) Geology, iv) NDVI (Rouse et al. 1974), v) plan curvature (Heerdegen and Beran 1982), vi) profile curvature (Heerdegen and Beran 1982), vii) Slope Steepness (Zevenbergen and Thorne 1987), viii) Tectonic, ix) Topographic Wetness Index (Beven and Kirkby 1979), and x) Use (Ballabio et al. 2016). The Geology, Aspect and Use predictors were coded as shown in Table 1.

Code	Geology	Aspect	Use
1	Sand and Gravel	North-North-East	Continuous urban fabric
2	Recent alluvial deposits	East-North-east	Sparsely vegetated areas
3	Conglomerates	East-South-East	Mixed forest
4	Paragneiss	South-South-East	-----
5	Arkosic clay marls	South-South-West	-----
6	Aplitic pegmatites	West-South-West	Mixed forest
7	Paragneiss to mica-schists	West-North-West	Citrus groves
8	Amphibolites	North-North-West	Complex cultivation patterns
9	Double micas marbles	-----	Grassland
10	Eluvial – colluvial horizon	-----	Olive groves

Table 1 – Categorical variable codes and correspondences.

3.2 Positives Dataset

The 137 landslides identified in the field were used to derive the point with the highest elevation along the corresponding polygon boundaries and subsequently generate Landslide Identification Points according to Cama et al. (2015) and Lombardo et al. (2014). Due to the limited number of cases, we adopted a circular diagnostic area (Rotigliano et al. 2011) or seed cell buffer (Dagdelenler et al. 2015) of 2.72m around each LIP to enable the increase in the size of the dataset and the investigation of a wider portion of the unstable landslide crowns. This operation ensures that the region responsible for the given landslide activation and the related geomorphological properties are brought into the modelling procedure. The chosen algorithm thereby learns how to discriminate instability conditions within the study area. On a synthetically generated 2m grid, coinciding with the HRDEM used to derive the topographic predictors, each centroid intersected by the chosen diagnostic area was exported to represent the region of space affected by instability. By doing so, the initial 137 LIPs divided into 54 *thin* and 83 *thick* became 375 and 573 positives, respectively. These unstable points were used as a dependent variable within the modelling procedure. Figure 6 shows the normalised univariate distribution of each predictor with respect to the two sets of unstable points. At this preliminary stage, it is already possible to recognise polarisation effects between the two landslide types with respect to the adopted predictors.

3.3 Statistical modelling and performance evaluation scheme

Statistical and data mining approaches have been readily applied for landslide susceptibility purposes proving their validity over the last three decades. However, their application has been bounded until recent times by methods relying on presence (landslide) and absence (no landslide) datasets. Analytical hierarchy process (Shahabi et al. 2014), Binary Logistic Regression (Conoscenti et al. 2016; Lombardo et al. 2014), Classification and Regression Trees (Stolle et al. 2015), Conditional Analysis (Vergari et al. 2011), Frequency Ratio (Kavzoglu et al. 2015), Fuzzy logic (Pourghasemi et al. 2012), Multivariate Adaptive Regression Spline (Conoscenti et al. 2015), Neural Network (Pardeshi et al. 2013), Random Forest (Trigila et al. 2015), Stochastic Gradient Treeboost (Lombardo et al. 2015) and Support Vector Machine (Su et al. 2015), all share a similar initial structure, where a balanced (Eker et al. 2015) or unbalanced (Heckmann et al.

2014) dataset is built by merging unstable and stable conditions for the given algorithm to be used to produce a susceptibility map. Despite the significant literature on the topic, there is still a substantial disagreement on how to construct the dataset to be modelled. In fact, part of the community, suggests the use of an equal number of pixels for landslide and no landslide areas (e.g. Suzen and Doyuran 2004; Yesilnacar and Topal 2005; Nefeslioglu et al. 2008), while many others scientific contributions propose an unequal proportions of positives and negatives (e.g. Atkinson and Massari 1998; Guzzetti et al. 1999; Can et al. 2005). Moving away from presence-absence methods, MaxEnt (Phillips and Dudík 2008) implements a presence-only or presence-background approach (Thibaud et al. 2014) by applying the Maximum Entropy principle (Jaynes 1957) to fit the model so that the estimated dependent distribution deviates from a uniform distribution as minimally as required to explain the observations (Gurutzeta et al. 2014). Recent applications (Convertino et al. 2013; Davis and Blesius 2015) of MaxEnt for landslide susceptibility mapping have demonstrated its utility, even in comparative studies (Felicísimo et al. 2013; Moosavi and Niazi 2015).

In this contribution the authors applied MaxEnt to produce landslide triggering-thickness susceptibility within the test catchment of Mili, using the presences of *thin* (crown thickness less than 1m) and *thick* (crown thickness equal or greater than 1m) landslides as a dependent variable.

Fifty models were generated by randomly selecting 75% of the original positives for calibration and 25% for validation. The goodness of fit and prediction skill of each replicate have been assessed through receiver operating characteristic (hereafter ROC) curves according to Phillips et al. (2006) and the corresponding area under the curve (AUC) values. It is worth mentioning that, distinct from presence-absence methods, MaxEnt must handle the absence of negative instances when building ROC curves as the False Positive rates (FP) cannot be computed. This is overcome by distinguishing presence from random, rather than presence from absence. As a consequence, a given ROC curve for landslide susceptibility purposes indicates the probability that, when drawing at random locations with presence and absence of landslides, the first case will have a higher predicted value than the second (Parolo et al. 2008). The aforementioned difference between presence-absence and presence-only methods in generating ROC curves is also reflected in the resulting AUC values. Table 2 compares the common performance-estimation thresholds for presence-absence cases (e.g. Binary Logistic Regression; Hosmer and Lemeshow 2000) with the corresponding values published for Maxent (Araujo and Guisan 2006).

	Binary Logistic Regression	**MaxEnt**
0.7-0.8	Acceptable	Average
0.8-0.9	Excellent	Good
0.9-1.0	Outstanding	Excellent

Table 2 . Difference between thresholds when evaluating the model score.

Predictive performances are not the only metric to assess the goodness of a model. Predictor contributions and roles represent a key step that should be used to assess the validity of a model for real-world geomorphological processes. In this contribution, we investigated this by means of: i) predictor importance (hereafter PI) or percentage contribution (Oke and Thompson 2015; Tien Bui et al. 2015), ii) jackknife tests (Shcheglovitova and Anderson 2013), and iii) response curves (Lombardo et al. 2015). The first metric represents the degree to which single covariates influence the final model, such that the percent contributions for all predictors in a model sum to 100% (Phillips, 2008). The second metric represents a test involving iterative generations of the models using the *j*-th variable only, as well as iteratively generating models using all but the *j*-th variable (Almalki et al. 2015). Each result is evaluated as a function of the corresponding AUC value, to consider the relative contribution of each predictor and the possible removal of non-improving covariates, with respect to the final output. This topic is particularly relevant when considering the Occam's Razor principle (Menzies 2014), which states that among equivalent model performances, one should opt for the model with the least complexity. The response curves show the probability of landslide occurrence in the domain of the *j*-th variable. Response curves may be plotted for single variable models or the full final models, allowing trends to be distinguished within small portions of the predictor domains that are positively or negatively correlated to the actual failures.

In order to evaluate the full modelling procedure, the precision (Giordano 1997) of the prediction needs to be taken into account, by assessing the uncertainty of the final landslide susceptibility maps. Precision represents the repeatability or reproducibility of the probability measurement across the fifty replicates. Several studies (e.g. Guzzetti et al. 2006; Rossi et al. 2010) analysed the mean probability of occurrence against standard deviation, at each of the cells partitioning the given area. This fundamental step provides a measure of the actual reliability of the landslide susceptibility map, distinguishing reliable sectors of the study area (where each of the fifty models produced the same

susceptibility values), from unreliable sectors (where the probability estimation has been unstable throughout the modelling procedure).

4. Results

Figure 7 shows the training and validation ROC curves for the two classes of landslide activations. Evaluation of both fitting and prediction skill, using the commonly used metric AUC (Fig. 8), shows the analyses produced excellent performances, following Araujo and Guisan (2006). The *thick* class produced average AUCs of 0.929 and 0.898, for calibration and test, respectively, while the *thin* class was characterized by 0.915 and 0.875, respectively. The associated variance proved to be extremely low, if not negligible during the calibration phase, with 0.005 and 0.009, standard deviation values for *thick* and *thin*, respectively. The standard deviation for the fifty test AUCs, was only slightly higher than the training, with 0.018 for the *thick* class and 0.033 for the *thin* class. This attested to strong stability throughout the multi-fold modelling procedure. Assuming reliable models were generated, both in terms of predictive performances and stable reproducibility, the contribution and role of the predictors were assessed in order to establish the geomorphologic validity of the results. Figure 9 represents the jack-knife tests (O'Banion and Olsen 2014) performed during the modelling phase. This plot summarises the AUC values obtained from the fifty replicates; the two mass movement classes are shown along the columns, and the rows contain the AUC values for single variable - models and full models with one variable absent. Different patterns arose between the two landslide classes, with slope and land use significant variables for the *thin* class. This is shown both in single variable - models with high AUCs and more strongly in the full models with one variable absent, where the absence of slope or land use negatively affected the overall predictive ability. Jack-knife tests represent a useful tool to analyse covariate interactions, making it possible to isolate redundant predictors. Profile and plan curvature seemed to be uncorrelated to the *thin* failures, as shown in the second quadrant, with both single variable - models located below the 0.5 or random prediction threshold. Conversely, for *thick* landslides, both curvatures appeared to be correlated to the mass movements. The NDVI, also appears to play an important role for the *thick* class, shown in Figure 10, by the percentage contribution of each covariate with respect to the full model.. This boxplot highlights Geology, NDVI, Slope and Land Use as being the main predictors for both landslide classes. However, the relative importance is shown to be significantly different for the two cases. In order to complete the assessment on the predictor behaviour within the modelling procedure, response curves (Lombardo et al. 2015) were calculated. These curves link the probability of occurrence against the domain of each predictor. Figure 11 shows the average response curves computed for the two landslide classes by superimposing the curves obtained by using just the *j*-th variable models with the curves obtained from the full models. The evaluation of landslide susceptibility precision was verified calculating the uncertainty of the probability estimations in the geographic space. Figure 12 shows the statistical moments of all the probability measurements for the two classes of mass movements, as the maximum, average and minimum susceptibilities, as well as the associated standard deviation. It is evident how the prediction distinguished different susceptible areas for *thick* and *thin* landslides. By intersecting the average susceptibility and its standard deviation it is possible to produce model-error plots. Figure 13 shows the values for each of the mapping units within the Mili catchment; these being approximately $1.4*10^6$ squared cells. This plot relates the two moments of the susceptibility distributions across the fifty replicates, while highlighting their univariate distribution. Using this, it is possible to infer how stable both types of landslide models were, with the majority of the prediction confined below 0.05 σ. The *thick* class appeared to be more stable than the *thin* class, as the standard deviation is unimodal and approximately centred at 0. Conversely, the standard deviation of the *thin* class has a bimodal distribution with one clear spike near zero and another near 0.05. Both landslide types appeared to behave similarly, with most of the Mili catchment predicted as stable. The *thick* class had a total of $9.7*10^4$ cells with a probability value greater than the 0.5 threshold, representing 6.7% of the whole catchment. The *thin* class had a total $8.3*10^4$ unstable cells, representing 5.7% of the study area.

To further investigate the spatial distribution of the susceptibility of each of the two classes, we superimposed the two maps. The two susceptibility maps were reclassified into two classes based on probability values: (i) 0 to 0.5 and (ii) 0.5 to 1. The two probability classes represented stable and unstable condition across the catchment of Mili. Combining values from the *thick* and *thin* susceptibility maps, for each of the mapping units, discriminated regions modelled in both cases as stable, from regions predicted unstable in both cases, as well as regions prone to generate just one of the two thicknesses at the crown. Figure 14 shows the combination of the *thick* and *thin* susceptibility maps highlighting how the prediction has worked differently for the two cases. In general, the hydrographic left is primarily controlled by *thick* landslide susceptibilities, whilst the hydrographic right is more susceptible to *thin* activations.

5. Discussion

In order to depict the spatial susceptibility of the two modelled classes of mass movements we adopted a presence-only method, together with a set of morphometric, geologic and vegetation predictors. While the predictors were chosen with reference to previous scientific studies on shallow landslide activations, the method we applied is novel. The geomorphological community has relied on presence-absence approaches since the early 1980's (e.g. Carrara 1983) and only a few very recent contributions have tested the MaxEnt presence-only method in the framework of landslide susceptibility studies (Convertino et al. 2013; Davis and Blesius 2015). Current literature focussing on landslide thickness at the apex, investigates the topic from a process-based (e.g. Anagnostopulos et al. 2015), analogical (e.g. Iverson, 2015) and deterministic perspectives (e.g. Avolio et al., 2013), with very few contributions of new statistical models (Posner and Georgakakos 2015).

The excellent model performances obtained in this study present a method for reliable interpretation of landslide thickness discriminant geomorphological (l.s.) effects. This interpretation was supported thanks to the stable reproducibility demonstrated across the multi-fold modelling procedure. Figure 10 highlighted how specific predictors played different roles, with respect to the two landslide classes. In fact, the overall predictive performance for the *thin* class was conditioned by at least 50%, just by the slope steepness. Conversely, the same parameter impacted the *thick* class to a lesser extent, accounting for just the 20% of the overall predictor importance. This indicates that other parameters and their coexistence are needed in order to establish the triggering conditions for greater volumes, while being steep alone, may lead a slope to fail as a shallow mass movement. Moreover, the slope angle threshold for landslide initiations significantly varies between the two classes. Figure 11 shows for *thin* mass movements an angle equal or greater than 40° is required to set the unstable condition, while for the other class the corresponding slope angle is equal or greater than 20°. The vegetation density, represented by NDVI, was important for both thickness classes, as the predominant covariate for the *thick* class (approximately 30% of PI) and the second covariate for the *thin* one (approximately 18%). In both cases, the absence of vegetation or relatively low greenness, contributed to the preconditions for landslide activations. This can be better interpreted by coupling with land use, which is the second contributor for the *thick* type and the third for the *thin* one (the PI being around 27% and 14%, respectively). Sparsely vegetated areas, are one of the three land use classes positively correlated with slope failure, more strongly for *thick* rather than the *thin* class. Similarly, landslide occurrence for both classes appeared to be sensitive to the spatial distribution of citrus groves, but was different for each class in case of olive groves. The olive grove class produced the highest susceptibility conditions among the other land uses for *thin* landslides, while it corresponded with stable conditions for the *thick* landslides. This is particularly interesting as the olive groves are suitable for planting on steep slopes and on shallow regolith overlying the bedrock (Gómez-Limón et al. 2012; Taguas et al. 2013). In addition to this, agricultural tilling practises (Palese et al. 2015) tend to remove grass or weed from the area neighbouring a given tree (Russo et al. 2015), thus exposing the bare soil to the rainfall discharges. Moreover, the leaf size and density for olive trees are known to be small in the Sicilian region, with a calculated Leaf Area Index of $1.2 m^2 m^{-2}$ at the canopy level (Rallo et al. 2014). This may impact the activation of shallow landslides in cases of heavy rainfall, because of minimal rain drop interception and consequent rain drop impact and splash effect (Kirby 1989), compared with other cultivations. The important predictors common to both thickness classes included the outcropping geology (PI of approximately 10 and 8% for *thick* and *thin*, respectively). The role of individual classes within this geological covariate is less clear because no common pattern characterises the two mass movements. Landslides with crowns with a thickness greater than one metre, were more likely in sand and gravel, arkosic clay marls and paragneiss lithologies. No relation was found between sand and gravel, or arkosic clay marls with the *thin* landslide class, and paragneiss showed only a weak association. Occurrence of landslides with *thin* crowns was strongly influenced by the presence of aplitic pegmatite, colluvial horizon and to a lesser extent, by conglomerate outcrops. This may be related to different processes of degradation between different lithotypes. Aspect and tectonic variables were not primary predictors, but they also played a role in the model for both mass movements. Aspect accounted for a PI of 6% and 3%, while distance from fault lines represented 0.5% and 2.5%, for *thick* and *thin*, respectively. SSE, SSW, WSW and WNW aspects increased susceptibility of both cases, more strongly for the *thick* rather than the *thin* landslides. In addition, ESE proved to be strongly correlated to *thin* landslide occurrence, but it marked stable conditions for the *thick* class. The distance from faults variable was markedly different for unstable/stable conditions between the two thickness classes. For *thin*, the length range of 0 to 50 metres from the fault lines produced unstable conditions, which suddenly shifted to strongly stable above 50 m. For *thick*, the inferred trend was also negative, but the distance range that characterised the unstable conditions was much longer and up to 500 metres. This can be interpreted as slope material properties changes with increased distance from the fault, because the fault array surrounding the main lineament, fractures the rock by an amount that is inversely proportional with respect to the distance from the lineament. Consequently, material proximal to the fault is more disintegrated and is mobilised more easily, resulting in the landslides that are more frequent and less thick. Conversely, relative further from a given fault, the material is less disintegrated and requires a stronger applied stress to be mobilised. This statement is supported by the fieldwork (landslide inventory) and also is reflected in the

higher number of failures in the *thick* class with respect to its counterpart. The *thin* landslides require a smaller activation threshold but their slope signatures fades faster with time. The spatial prediction of *thick* and *thin* landslides, in the two susceptibility maps reflects geographic relationships to faults described above. *Thick* failures were mostly confined to the hydrologic left, while the opposite situation characterised the *thin* class. This has been interpreted as due to the tectonic settings together with the angle between the slope bedding, the joint system, the schistosity and the direction of the ground surface slopes. All these features influenced the characteristics of the debris cover (i.e. typology and thickness) giving rise to different slope responses recorded into the two landslide sets. Combining results produced in this research, showed slope steepness and vegetation were the most important predisposing factors. Although these parameters are present across the catchment, slope susceptibility to failure was decided by contributions from the other destabilising factors.

Looking at published methodological literature beyond landslide studies, soil thickness prediction at the catchment scale (e.g. Catani et al. 2010; Tesfa et al. 2009), requires similar fieldwork activities and statistical analyses. The present work draws on these studies for landslide susceptibility. The most common approaches for assessing the validity of landslide susceptibility models do not usually include jack-knife test and response curves. However, the authors believe this test to be effective, comprehensive and simple for interpretation when compared to common practises such as predictor ranking and predictor coefficients evaluations (e.g. Costanzo et al. 2014; Mathew et al. 2009). Predictor ranking provides a more static view with respect to the jack-knife tests and similarly, the coefficients of each covariate do not consider specific portions of the predictor domains, which is possible when computing the response curves.

The present work may be positioned among various recent contributions centred on landslide susceptibility in the north-easternmost sector of Sicily (e.g. Ciampalini et al. 2015). The work is distinct because most of papers have analysed the area to the south, where most damages occurred during the 2009 disaster; including the catchments of Giampilieri (Del Ventisette et al. 2012; Lombardo et al. 2014), Briga (Lombardo et al. 2015; Schilirò et al. 2015), Itala (Cama et al. 2015; Trigila et al. 2015), with only one study including the Mili catchment (Zini et al., 2015). Similarities may be drawn between this study and the others in the area, as the land use (Reichenbach et al. ,2014), the tectonic effects (De Guidi and Scudero, 2013), slope (Penna et al., 2014) and the vegetation (Reichenbach et al.,2015) have been proven to alter landslide susceptibility, even if the landslide inventory was treated differently. The contribution from Zini et al. (2015) has focussed on the erodibility index as a proxy for susceptibility. The methodology was different, however the number and types of landslides were analogously recognised but geographical susceptibility areas in the central portion of the catchment was also recognised to be more prone than the rest.

6. Conclusions

The approach described in this contribution highlights the value of free accessible reliable spatial data and the requirement of minimal fieldwork to define landslide susceptibility. Several contributions have shown that landslide inventories may be digitised from Google Earth (e.g. Costanzo et al. 2012; Van Den Eeckhaut et al. 2012; Zhang et al. 2015) and the covariates for modelling may be obtained from satellite imagery (e.g. Ahmed 2015; Brocca et al. 2012; Stolle et al. 2015), thus, setting the base for robust spatial predictive models by remote data collection. These methods reduce the need for expensive, time demanding fieldwork for studies at a catchment scale. Although remote methods are available, the authors have shown in this study that field data collection of specific attributes can significantly improve the landslide susceptibility model and its interpretation within a given catchment. Measurements of landslide crown thickness onsite, trains statistical models to distinguish between the susceptibility of landslides in *thick* or *thin* layers of the regolith depending on local environmental predictor variables. This is significant because it may be considered an indicator of the potential magnitude of a future landslide. A greater volume detached from the crown area translates to a greater moving mass, and an elevated entrainment capacity while incising the slope during transport; thereby leading to longer travel distances. All numerical methods, these being either continuous, discontinuous or hybrid (Hungr et al. 2005) confer this physical reasoning, assuming constant boundary conditions between different triggering locations. Landslide susceptibility that considers the volume of slope material destabilised, is useful for landslide risk assessment and planning.

Landslide studies aim to identify areas with a greater probability of being hit by a given landslide and of a given magnitude. This is the core difference between landslide susceptibility (e.g. Kritikos and Davies 2015) and hazard, where the latter should also include the probability of mobilising the total volume for a given failure. This study modelled the probability of mobilising a given volume only at the apex and may be considered a move towards landslide hazard assessment rather than a classic susceptibility study.

The Maxent approach produced excellent predictions, while also discriminating between different failure mechanisms. Together with an exhaustive analysis of the model performances and their associated reproducibility, the adoption of a comprehensive evaluation of the predictor roles enabled specific interpretations of the triggering effects between different activation types. This has been achieved by combining, predictor importance, jack-knife tests and response curves, which the authors consider to be the current most effective way to assess geomorphological (l.s.) validity of the models from not just the statistical, but also geological and application standpoint.

7. Acknowledgements

The authors would like to acknowledge the efforts of Melanie Froude, Postdoctoral researcher at the University of East Anglia, for editing this manuscript to improve its readability.

8. Reference

Ahmed B (2015) Landslide susceptibility modelling applying user-defined weighting and data-driven statistical techniques in Cox's Bazar Municipality, Bangladesh. Natural Hazards 79(3):1707-1737. doi: 10.1007/s11069-015-1922-4

Aldega L, Corrado S, Paolo LD, Somma R, Maniscalco R, Balestrieri ML (2011) Shallow burial and exhumation of the Peloritani Mountains (NE Sicily, Italy): Insight from paleothermal and structural indicators. Bulletin of the Geological Society of America 123(1-2):132-149. doi: 10.1130/B30093.1

Almalki M, Alrashidi M, O'Connell MJ, Shobrak M, Székely T (2015) Modelling the distribution of wetland birds on the Red Sea coast in the Kingdom of Saudi Arabia. Applied Ecology and Environmental Research, 13 (1), pp. 67-84. doi: 10.15666/aeer/1301_067084

Anagnostopoulos GG, Fatichi S, Burlando P (2015) An advanced process-based distributed model for the investigation of rainfall-induced landslides: The effect of process representation and boundary conditions. Water Resources Research, 51 (9), pp. 7501-7523.

Atkinson PM, Massari R (1998) Generalised linear modelling of susceptibility to landsliding in the central Apennines, Italy. Computers & Geosciences 24(4):373-385. doi: 10.1016/S0098-3004(97)00117-9

Avolio MV, Di Gregorio S, Lupiano V, Mazzanti P (2013) SCIDDICA-SS3: A new version of cellular automata model for simulating fast moving landslides. Journal of Supercomputing 65(2):682-696. doi: 10.1007/s11227-013-0948-1

Ballabio C, Panagos P, Monatanarella L (2016) Mapping topsoil physical properties at European scale using the LUCAS database. Geoderma 261:110-123

Bradley BA (2015) Predicting abundance with presence-only models. Landscape Ecology 12 p. Article in Press. doi: 10.1007/s10980-015-0303-4

Brocca L, Ponziani F, Moramarco T, Melone F, Berni N, Wagner W (2012) Improving landslide forecasting using ASCAT-derived soil moisture data: A case study of the Torgiovannetto landslide in central Italy. Remote Sensing 4(5):1232-1244. doi: 10.3390/rs4051232

Cama M, Lombardo L, Conoscenti C, Agnesi V, Rotigliano E (2015) Predicting storm-triggered debris flow events: Application to the 2009 Ionian Peloritan disaster (Sicily, Italy). Natural Hazards and Earth System Sciences 15(8):1785-1806. doi: 10.5194/nhess-15-1785-2015

Cama M, Conoscenti C, Lombardo L, Rotigliano E, (2016) Exploring relationships between pixel size and accuracy for debris flow susceptibility models: a test in the Giampilieri catchment (Sicily, Italy). Earth and Environmental Sciences, 75 (3), art. no. 238, pp. 1-21. DOI: 10.1007/s12665-015-5047-6

Can T, Nefeslioglu HA, Gokceoglu C, Sonmez H, Duman TY (2005) Susceptibility assessments of shallow earthflows triggered by heavy rainfall at three catchments by logistic regression analyses. Geomorphology 72(1–4):250-271. doi: 10.1016/j.geomorph.2005.05.011

Capitani M, Ribolini A, Federici PR (2013) Influence of deep-seated gravitational slope deformations on landslide distributions: A statistical approach. Geomorphology 201:127-134. doi: 10.1016/j.geomorph.2013.06.014

Carafa MMC, Barba S, Bird P (2015) Neotectonics and long-term seismicity in Europe and the Mediterranean region. Journal of Geophysical Research B: Solid Earth 120(7):5311-5342. doi: 10.1002/2014JB011751

Carrara A (1983) Multivariate models for landslide hazard evaluation. Mathematical Geology, 15(3):403-427. DOI: 10.1007/BF01031290

Catani F, Segoni S, Falorni G (2010) An empirical geomorphology-based approach to the spatial prediction of soil thickness at catchment scale. Water Resources Research, 46 (5). DOI: 10.1029/2008WR007450

Ciampalini A, Raspini F, Bianchini S, Frodella W, Bardi F, Lagomarsino D, Di Traglia F, Moretti S, Proietti C, Pagliara P, Onori R, Corazza A, Duro A, Basile G, Casagli N (2015) Remote sensing as tool for development of landslide databases: The case of the Messina Province (Italy) geodatabase. Geomorphology, 249, pp. 103-118. DOI: 10.1016/j.geomorph.2015.01.029

Comerci V, Vittori E, Blumetti AM, Brustia E, Di Manna P, Guerrieri L, Lucarini M, Serva L (2015) Environmental effects of the December 28, 1908, Southern Calabria–Messina (Southern Italy) earthquake. Natural Hazards 76(3):1849-1891. doi: 10.1007/s11069-014-1573-x

Conoscenti C, Ciaccio M, Caraballo-Arias NA, Gómez-Gutiérrez T, Rotigliano E, Agnesi V (2015) Assessment of susceptibility to earth-flow landslide using logistic regression and multivariate adaptive regression splines: A case of the Belice River basin (western Sicily, Italy) Geomorphology 242:49-64. doi: 10.1016/j.geomorph.2014.09.020

Conoscenti C, Rotigliano E, Cama M, Caraballo-Arias NA, Lombardo L, Agnesi V (2016) Exploring the effect of absence selection on landslide susceptibility models: A case study in Sicily, Italy. Geomorphology, 261, pp. 222-235. doi: 10.1016/j.geomorph.2016.03.006

Convertino M, Troccoli A, Catani F (2013) Detecting fingerprints of landslide drivers: A MaxEnt model. Journal of Geophysical Research: Earth Surface 118(3):1367-1386. doi: 10.1002/jgrf.20099

Costanzo D, Cappadonia C, Conoscenti C, Rotigliano E (2012) Exporting a Google Earth™ aided earth-flow susceptibility model: A test in central Sicily. Natural Hazards 61(1):103-114. doi: 10.1007/s11069-011-9870-0

Costanzo D, Chacón J, Conoscenti C, Irigaray C, Rotigliano E (2014) Forward logistic regression for earth-flow landslide susceptibility assessment in the Platani river basin (southern Sicily, Italy). Landslides, 11 (4), pp. 639-653. DOI: 10.1007/s10346-013-0415-3

Dagdelenler G, Nefeslioglu HA, Gokceoglu C (2015) Modification of seed cell sampling strategy for landslide susceptibility mapping: an application from the Eastern part of the Gallipoli Peninsula (Canakkale, Turkey). Bulletin of Engineering Geology and the Environment, 16 p. Article in Press. DOI: 10.1007/s10064-015-0759-0

Davis J, Blesius L (2015) A hybrid physical and maximum-entropy landslide susceptibility model. Entropy 17(6):4271-4292. doi: 10.3390/e17064271

De Guidi G, Scudero S (2013) Landslide susceptibility assessment in the Peloritani Mts. (Sicily, Italy) and clues for tectonic control of relief processes. Natural Hazards and Earth System Science 13(4):949-963. doi: 10.5194/nhess-13-949-2013

Del Ventisette C, Garfagnoli F, Ciampalini A, Battistini A, Gigli G, Moretti S, Casagli N (2012) An integrated approach to the study of catastrophic debris-flows: Geological hazard and human influence. Natural Hazards and Earth System Science, 12 (9), pp. 2907-2922. DOI: 10.5194/nhess-12-2907-2012

Dickson ME, Perry GLW (2015) Identifying the controls on coastal cliff landslides using machine-learning approaches. Environmental Modelling and Software. Article in Press. doi: 10.1016/j.envsoft.2015.10.029

Di Stefano P, Favara R, Luzio D, Renda P, Cacciatore MS, Calò M, Napoli G, Parisi L, Todaro S, Zarcone G (2015) A regional-scale discontinuity in western Sicily revealed by a multidisciplinary approach: A new piece for understanding the geodynamic puzzle of the southern Mediterranean. Tectonics, Article in Press. DOI: 10.1002/2014TC003759

Eker AM, Dikmen M, Cambazoğlu S, Düzgün ŞHB, Akgün H (2015) Evaluation and comparison of landslide susceptibility mapping methods: a case study for the Ulus district, Bartın, northern Turkey. International Journal of Geographical Information Science 29(1):132-158. doi: 10.1080/13658816.2014.953164

Felicísimo ÁM, Cuartero A, Remondo J, Quirós E (2013) Mapping landslide susceptibility with logistic regression, multiple adaptive regression splines, classification and regression trees, and maximum entropy methods: A comparative study. Landslides 10(2):175-189. doi: 10.1007/s10346-012-0320-1

Giordano JL (1997) On the sensitivity, precision and resolution in DC Wheatstone bridges. European Journal of Physics, 18(1), 22-27.

Giunta G, Gueli AM, Monaco C, Orioli S, Ristuccia GM, Stella G, Troja SO (2012) Middle-Late Pleistocene marine terraces and fault activity in the Sant'Agata di Militello coastal area (north-eastern Sicily). Journal of Geodynamics 55:32-40. doi: 10.1016/j.jog.2011.11.005

Gómez-Limón JA, Picazo-Tadeo AJ, Reig-Martínez E (2012) Eco-efficiency assessment of olive farms in Andalusia. Land Use Policy 29(2):395-406. doi: 10.1016/j.landusepol.2011.08.004

Guzzetti F, Carrara A, Cardinali M, Reichenbach P (1999) Landslide hazard evaluation: an aid to a sustainable development. Geomorphology 31:181-216

Guzzetti F, Reichenbach P, Ardizzone F, Cardinali M, Galli M (2006) Estimating the quality of landslide susceptibility models. Geomorphology 81(1-2):166-184

Hand DJ, Till RJ (2001) A Simple Generalisation of the Area Under the ROC Curve for Multiple Class Classification Problems. Machine Learning 45(2):171-186

Harders R, Ranero CR, Weinrebe W, Behrmann JH (2011) Submarine slope failures along the convergent continental margin of the Middle America Trench. Geochemistry, Geophysics, Geosystems 12(6), art. no. Q05S3. doi: 10.1029/2010GC003401

Heckmann T, Gegg K, Gegg A, Becht M (2014) Sample size matters: investigating the effect of sample size on a logistic regression susceptibility model for debris flows. Nat Hazards Earth Sys 14:259–278. doi:10.5194/nhess-14-259-2014, 2014

Hudak AT, Robichaud P, Evans JS, Clark J, Lannom K, Morgan P, Stone C (2004) Field validation of Burned Area Reflectance Classification (BARC) products for post fire assessment. – University of Nebraska, Lincoln, NE, USA.

Hungr O, Corominas J, Eberhardt E (2005) Estimating landslide motion mechanisms, travel distance and velocity". In Hungr O, Fell R, Couture R, Eberthardt E (editors) Landslide Risk Management. Taylor and Francis, London, pp. 99-128

Iovine GGR, Greco R, Gariano, SL, Pellegrino AD, Terranova OG (2014) Shallow-landslide susceptibility in the Costa Viola mountain ridge (southern Calabria, Italy) with considerations on the role of causal factors. Natural Hazards 73(1):111-136

Iverson RM (2015) Scaling and design of landslide and debris-flow experiments. Geomorphology, 244, pp. 9-20. DOI: 10.1016/j.geomorph.2015.02.033

Kavzoglu T, Kutlug Sahin E, Colkesen I (2015) An assessment of multivariate and bivariate approaches in landslide susceptibility mapping: a case study of Duzkoy district. Natural Hazards 76(1):471-496. doi: 10.1007/s11069-014-1506-8

Kirkby MJ (1989) A model to estimate the impact of climatic change on hillslope and regolith form. Catena 16(4-5):321-341. doi: 10.1016/0341-8162(89)90018-0

Kirschbaum DB, Stanley T, Simmons J (2015) A dynamic landslide hazard assessment system for Central America and Hispaniola. Natural Hazards and Earth System Sciences, 15 (10), pp. 2257-2272. DOI: 10.5194/nhess-15-2257-2015

Köthe R, Lehmeier F (1993) SARA - Ein Programmsystem zur Automatischen Relief-Analyse. - Standort - Z. f. Angewandte Geographie 4/93:11-21

484 Kritikos T, Davies T (2015) Assessment of rainfall-generated shallow landslide/debris-flow susceptibility and runout
485 using a GIS-based approach: application to western Southern Alps of New Zealand. Landslides, 12 (6), pp. 1051-1075.
486 DOI: 10.1007/s10346-014-0533-6

487 Lentini F, Carbone S, Messina A (2007) Carta Geologica d'Italia scala 1:50.000 Foglio 601 "Messina-Reggio di
488 Calabria", con note illustrative. Apat Agenzia per la protezione dell'ambiente e per i servizi tecnici, Dipartimento
489 Difesa del Suolo – Servizio geologico d'Italia.
490 http://www.isprambiente.gov.it/Media/carg/note_illustrative/601_Messina_Reggio_Calabria.pdf

491 Lombardo L, Cama M, Maerker M, Rotigliano E (2014) A test of transferability for landslides susceptibility models
492 under extreme climatic events: Application to the Messina 2009 disaster. Natural Hazards, 74 (3), pp. 1951-1989. DOI:
493 10.1007/s11069-014-1285-2

494 Lombardo L, Cama M, Conoscenti C, Märker M, Rotigliano E (2015) Binary logistic regression versus stochastic
495 gradient boosted decision trees in assessing landslide susceptibility for multiple-occurring landslide events: application
496 to the 2009 storm event in Messina (Sicily, southern Italy). Natural Hazards, 79 (3), pp. 1621-1648. DOI:
497 10.1007/s11069-015-1915-3

498 Massari F, Prosser G (2013) Late Cenozoic tectono-stratigraphic sequences of the Crotone Basin: Insights on the
499 geodynamic history of the Calabrian arc and Tyrrhenian Sea. Basin Research 25(1):26-51. doi: 10.1111/j.1365-
500 2117.2012.00549.x

501 Mathew J, Jha VK, Rawat GS (2009) Landslide susceptibility zonation mapping and its validation in part of Garhwal
502 Lesser Himalaya, India, using binary logistic regression analysis and receiver operating characteristic curve method.
503 Landslides, 6 (1), pp. 17-26. DOI: 10.1007/s10346-008-0138-z

504 Menzies T (2014) Occam's razor and simple software project management. In Ruhe G, Wohlin C (editors) Software
505 Project Management in a Changing World. Springer-Verlag, Berlin Heidelberg, pp 447-472

506 Merow C, Smith MJ, Silander JA (2013) A practical guide to MaxEnt for modeling species' distributions: What it does,
507 and why inputs and settings matter. Ecography 36(10):1058-1069

508 Moosavi V, Niazi Y (2015) Development of hybrid wavelet packet-statistical models (WP-SM) for landslide
509 susceptibility mapping. Landslides 18 p. Article in Press. doi: 10.1007/s10346-014-0547-0

510 Nefeslioglu HA, Gokceoglu C, Sonmez H (2008) An assessment on the use of logistic regression and artificial neural
511 networks with different sampling strategies for the preparation of landslide susceptibility maps. Engineering Geology
512 97(3-4):171-191

513 O'Banion MS, Olsen MJ (2014) Predictive seismically-induced landslide hazard mapping in oregon using a maximum
514 entropy model (MaxEnt). Proceedings of the 10th National Conference in Earthquake Engineering, Earthquake
515 Engineering Research Institute, Anchorage, AK, 2014

516 Oke OA, Thompson KA (2015) Distribution models for mountain plant species: The value of elevation. Ecological
517 Modelling 301:72-77

518 Palese AM, Ringersma J, Baartman JEM, Peters P, Xiloyannis C (2015) Runoff and sediment yield of tilled and
519 spontaneous grass-covered olive groves grown on sloping land. Soil Research 53(5):542-552. doi: 10.1071/SR14350

520 Penna D, Borga M, Aronica GT, Brigandì G, Tarolli P (2014) The influence of grid resolution on the prediction of
521 natural and road-related shallow landslides. Hydrology and Earth System Sciences, 18 (6), pp. 2127-2139. DOI:
522 10.5194/hess-18-2127-2014

523 Petschko H, Brenning A, Bell R, Goetz J, Glade T (2014) Assessing the quality of landslide susceptibility maps - Case
524 study Lower Austria. Nat Hazards Earth Sys 14(1):95-118. doi: 10.5194/nhess-14-95-2014

525 Phillips SJ, Anderson RP, Schapire RE (2006) Maximum entropy modelling of species geographic distributions.
526 Ecological Modelling 190:231–259

527 Phillips SJ, Dudík M (2008) Modeling of species distributions with Maxent: New extensions and a comprehensive
528 evaluation. Ecography 31(2):161-175. doi: 10.1111/j.0906-7590.2008.5203.x

529 Phillips S (2008) A brief tutorial on MaxEnt. AT&T Res. www.cs.princeton.edu/~schapire/maxent/tutorial/tutorial.doc)

530 Posner AJ, Georgakakos KP (2015) Soil moisture and precipitation thresholds for real-time landslide prediction in El
531 Salvador. Landslides, 12 (6), pp. 1179-1196. DOI: 10.1007/s10346-015-0618-x

532 Pourghasemi HR, Pradhan B, Gokceoglu C (2012) Application of fuzzy logic and analytical hierarchy process (AHP) to
533 landslide susceptibility mapping at Haraz watershed. Iran Natural Hazards 63(2):965-996. doi: 10.1007/s11069-012-
534 0217-2

535 Procter DS, Cottrell J, Watts K, Robinson EJH (2015) Do non-native conifer plantations provide benefits for a native
536 forest specialist, the wood ant Formica lugubris? Forest Ecology and Management 357:22-32. doi:
537 10.1016/j.foreco.2015.07.034

538 Rallo G, Minacapilli M, Ciraolo G, Provenzano G (2014) Detecting crop water status in mature olive groves using
539 vegetation spectral measurements. Biosystems Engineering 128:52-68. doi: 10.1016/j.biosystemseng.2014.08.012

540 Reichenbach P, Busca C, Mondini AC, Rossi M (2014) The Influence of Land Use Change on Landslide Susceptibility
541 Zonation: The Briga Catchment Test Site (Messina, Italy). Environmental Management, 54 (6), pp. 1372-1384. DOI:
542 10.1007/s00267-014-0357-0

543 Reichenbach P, Mondini AC, Rossi M (2015) Land use change scenarios and landslide susceptibility zonation: The
544 briga catchment test area (Messina, Italy). Engineering Geology for Society and Territory - Volume 1: Climate Change
545 and Engineering Geology, pp. 557-561. DOI: 10.1007/978-3-319-09300-0_104

546 Rossi M, Guzzetti F, Reichenbach P, Mondini AC, Peruccacci S (2010) Optimal landslide susceptibility zonation based
547 on multiple forecasts. Geomorphology 114(3):129-142Rotigliano E, Agnesi V, Cappadonia C, Conoscenti C (2011) The
548 role of the diagnostic areas in the assessment of landslide susceptibility models: A test in the sicilian chain. Natural
549 Hazards 58(3):981-999. doi: 10.1007/s11069-010-9708-1

550 Russo G, Vivaldi GA, De Gennaro B, Camposeo S (2015) Environmental sustainability of different soil management
551 techniques in a high-density olive orchard. Journal of Cleaner Production 107:498-508. doi:
552 10.1016/j.jclepro.2014.06.064

553 Schilirò L, Esposito C, Scarascia Mugnozza G (2015) Evaluation of shallow landslide-triggering scenarios through a
554 physically based approach: An example of application in the southern Messina area (northeastern Sicily, Italy). Natural
555 Hazards and Earth System Sciences, 15 (9). DOI: 10.5194/nhess-15-2091-2015Shahabi H, Khezri S, Ahmad BB,
556 Hashim M (2014) Landslide susceptibility mapping at central Zab basin, Iran: A comparison between analytical
557 hierarchy process, frequency ratio and logistic regression models. Catena 115:55-70. doi: 10.1016/j.catena.2013.11.014

558 Stolle A, Langer M, Blöthe JH, Korup O (2015) On predicting debris flows in arid mountain belts. Global and Planetary
559 Change 126:1-13. doi: 10.1016/j.gloplacha.2014.12.005

560 Shcheglovitova M, Anderson RP, (2013) Estimating optimal complexity for ecological niche models: A jackknife
561 approach for species with small sample sizes. Ecological Modelling 269:9-17

562 Stolle A, Langer M, Blöthe JH, Korup O (2015) On predicting debris flows in arid mountain belts. Global and Planetary
563 Change 126:1-13. doi: 10.1016/j.gloplacha.2014.12.005

564 Su C, Wang L, Wang X, Huang Z, Zhang X (2015) Mapping of rainfall-induced landslide susceptibility in Wencheng,
565 China, using support vector machine. Natural Hazards 76(3):1759-1779. doi: 10.1007/s11069-014-1562-0

566 Süzen ML, Doyuran V (2004) A comparison of the GIS based landslide susceptibility assessment methods: Multivariate
567 versus bivariate. Environmental Geology 45(5):665-679

568 Tagil S, Jenness J, (2008) GIS-Based Automated Landform Classification and Topographic, Landcover and Geologic
569 Attributes of Landforms Around the Yazoren Polje, Turkey. Journal of Applied Sciences 8:910-921. DOI:
570 10.3923/jas.2008.910.921

571 Taguas EV, Ayuso JL, Pérez R, Giráldez JV, Gómez JA (2013) Intra and inter-annual variability of runoff and sediment
572 yield of an olive micro-catchment with soil protection by natural ground cover in Southern Spain. Geoderma 206:49-62.
573 doi: 10.1016/j.geoderma.2013.04.011

574 Tesfa TK, Tarboton DG, Chandler DG, McNamara JP (2009) Modeling soil depth from topographic and land cover
575 attributes. Water Resources Research, 45 (10), art. no. W10438. DOI: 10.1029/2008WR007474

576 Tien Bui D, Tuan TA, Klempe H, Pradhan B, Revhaug I (2015) Spatial prediction models for shallow landslide
577 hazards: a comparative assessment of the efficacy of support vector machines, artificial neural networks, kernel logistic
578 regression, and logistic model tree. Landslides 18 p. Article in Press. doi: 10.1007/s10346-015-0557-6

579 Trigila A, Iadanza C, Esposito C, Scarascia-Mugnozza G (2015) Comparison of Logistic Regression and Random
580 Forests techniques for shallow landslide susceptibility assessment in Giampilieri (NE Sicily, Italy) Geomorphology.
581 Article in Press.

582 Van Den Eeckhaut M, Hervás J, Jaedicke C, Malet JP, Montanarella L, (2012) Nadim F. Statistical modelling of
583 Europe-wide landslide susceptibility using limited landslide inventory data. Landslides 9(3):357-369. doi:
584 10.1007/s10346-011-0299-z

585 West AM, Kumar S, Jarnevich CS (2015) Regional modeling of large wildfires under current and potential future
586 climates in Colorado and Wyoming, USA. Climatic Change 13 p. Article in Press. doi: 10.1007/s10584-015-1553-5

587 Yesilnacar E, Topal T (2005) Landslide susceptibility mapping: A comparison of logistic regression and neural
588 networks methods in a medium scale study, Hendek region (Turkey). Engineering Geology 79(3-4):251-266. doi:
589 10.1016/j.enggeo.2005.02.002

590 Zevenbergen LW, Thorne CR (1987) Quantitative analysis of land surface topography. Earth Surface Processes and
591 Landforms 12:47-56

592 Zhang J, Gurung DR, Liu R, Murthy MSR, Su F (2015) Abe Barek landslide and landslide susceptibility assessment in
593 Badakhshan Province, Afghanistan. Landslides 12(3)597-609. doi: 10.1007/s10346-015-0558-5

594 Zini A, Grauso S, Verrubbi V, Falconi L, Leoni G, Puglisi C (2015) The RUSLE erosion index as a proxy indicator for
595 debris flow susceptibility. Landslides, 12 (5), pp. 847-859. DOI: 10.1007/s10346-014-0515-8

596

597 Captions

598 Figure 1 - General settings of the area and the study area in the red rectangle (a) (modified from Di Stefano et al., 2015).
599 Focus on the study area overlying the DEM, outcropping lithologies and tectonic lineaments (b) (modified from Lentini
600 et al., 2007).

601 Figure 2 - Outcropping lithologies recognised during fieldwork. One metre thick colluvial horizon with angular
602 metamorphosed clasts in a clayey/sandy matrix (a). Recent clast-supported alluvial deposit, this being non-cemented,
603 including angular clasts and pelitic levels (b). Sand and gravel layered in a sandy matrix (c). Fractured conglomerate
604 (d). Marl in a clayey matrix, fractured in prismatic wedges and including muscovite and mafic clasts (e). Augen gneiss
605 (f). Micashist with leucosomatic patches (g). Clay layers interbedded to sandy levels (h).

606 Figure 3 – Precipitation records from the St. Stefano Briga rain gauge during the major events within the considered
607 timeframe.

608 Figure 4 – Metric metamorphic blocks detached due to a fall (a). Deep-seated rotational slide with smaller associated
609 debris flows (b). Minor fissures inside the aforementioned rotational slide (c). Landslide deposit with recent vegetation
610 (d). Debris slide propagating as debris avalanche (e). Debris flow fortunately channeling before reaching the settlements
611 at the foothill (f).

612 Figure 5 – Histogram of crown thicknesses among the debris slides and flows recognised in the catchment (a).
613 Distribution of crown thicknesses within the catchment, these being reclassified into thin and thick groups (b).

614 Figure 6 – Subplot showing the values of each predictors with respect to the two considered landslide classes, these
615 being shown in red (thin) and blue (thick).

616 Figure 7 – ROC curves calculated both during calibration (grey) and validation (coloured) phases for both landslide
617 types, red for thin and blue for thick. Lighter colours represent the confidence interval measured in one standard
618 deviation.

619 Figure 8 – AUC values obtained through the fifty replicates for the two landslide classes (red for thin and blue for thick)
620 both for training (circles) and test (squares).

Figure 9 – Boxplot of the jack-knife tests for both landslide types across the fifty replicates by calculating the AUC from single-variable models and all but one variable models. Red lines represent the median, the edges of the box are the 25th and 75th percentiles, upper and lower whiskers extend to the most extreme AUC not considered outliers, red crosses are the actual outliers. Dotted lines represent the average test AUC obtained across the fifty replicates for each of the two classes.

Figure 10 – Boxplot of predictor importances (PI) for each of the ten selected predictors. Red lines represent the median, the edges of the box are the 25th and 75th percentiles, upper and lower whiskers extend to the most extreme PI not considered outliers, red crosses are the actual outliers.

Figure 11 – Subplot showing response curves for the ten adopted predictors. Continuous lines or filled circles show the full model response curves whilst the dotted lines or empty squares show the single variable model response curves. The red colour represents the *thin* class and the blue one represents the *thick* class.

Figure 12 – Max, average, min landslide susceptibilities and their confidence interval measured in one standard deviation are shown for the whole catchment and for the two thickness classes.

Figure 13 – Model error shown through scatterhist plots for the two thickness classes. The average susceptibilities for each pixel in the catchment are plotted against the corresponding standard deviation. The histograms present the univariate distribution of x and y whilst the black lines are the best quadratic fit.

Figure 14 – Combined triggering-thickness susceptibilty map for the catchment of the Mili stream.

Fig.1

Click here to download Figure Fig1_31.03.2016.jpg

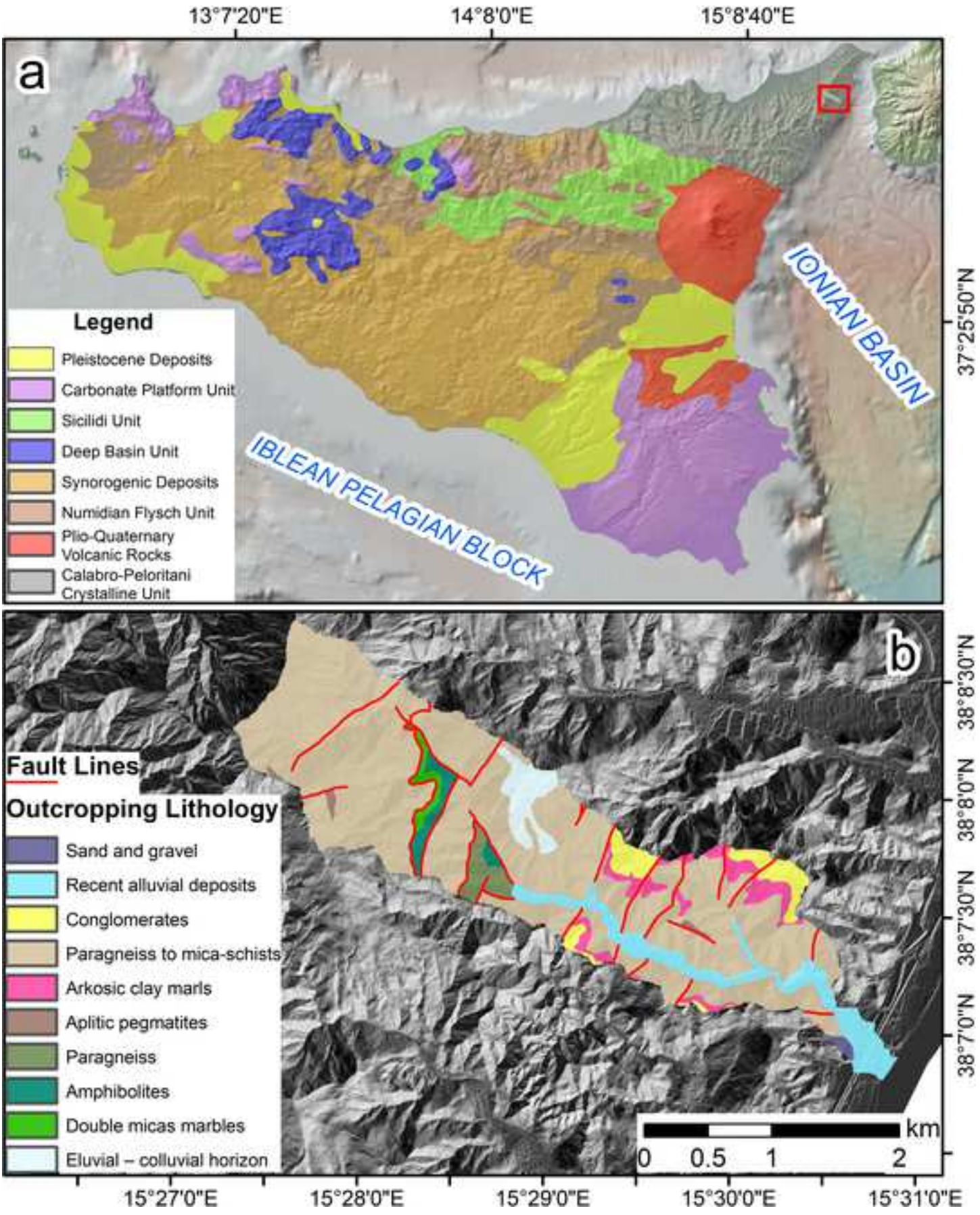

Fig.2

Click here to download Figure fig2.tif

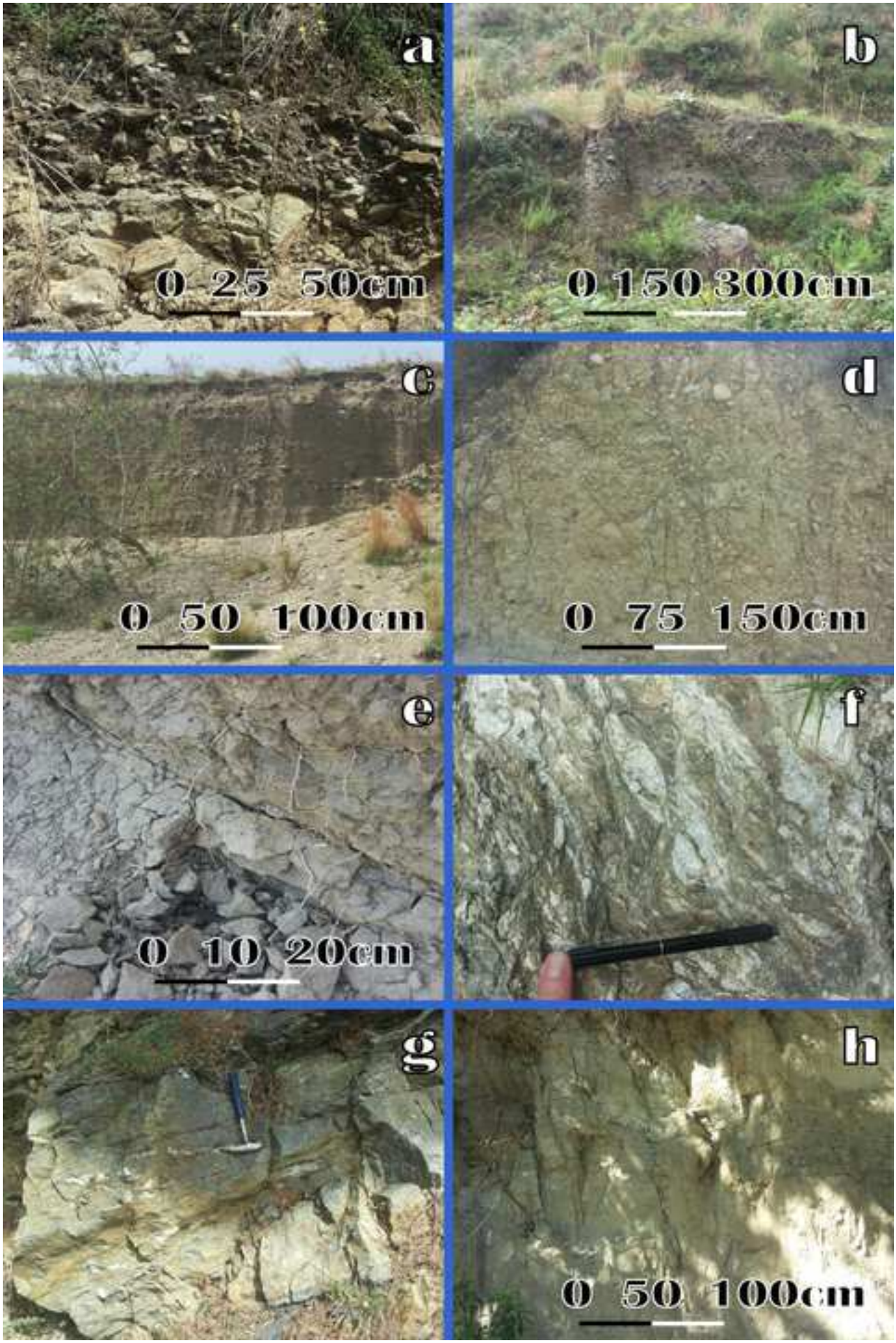

Fig.3

Click here to download Figure fig3.tif

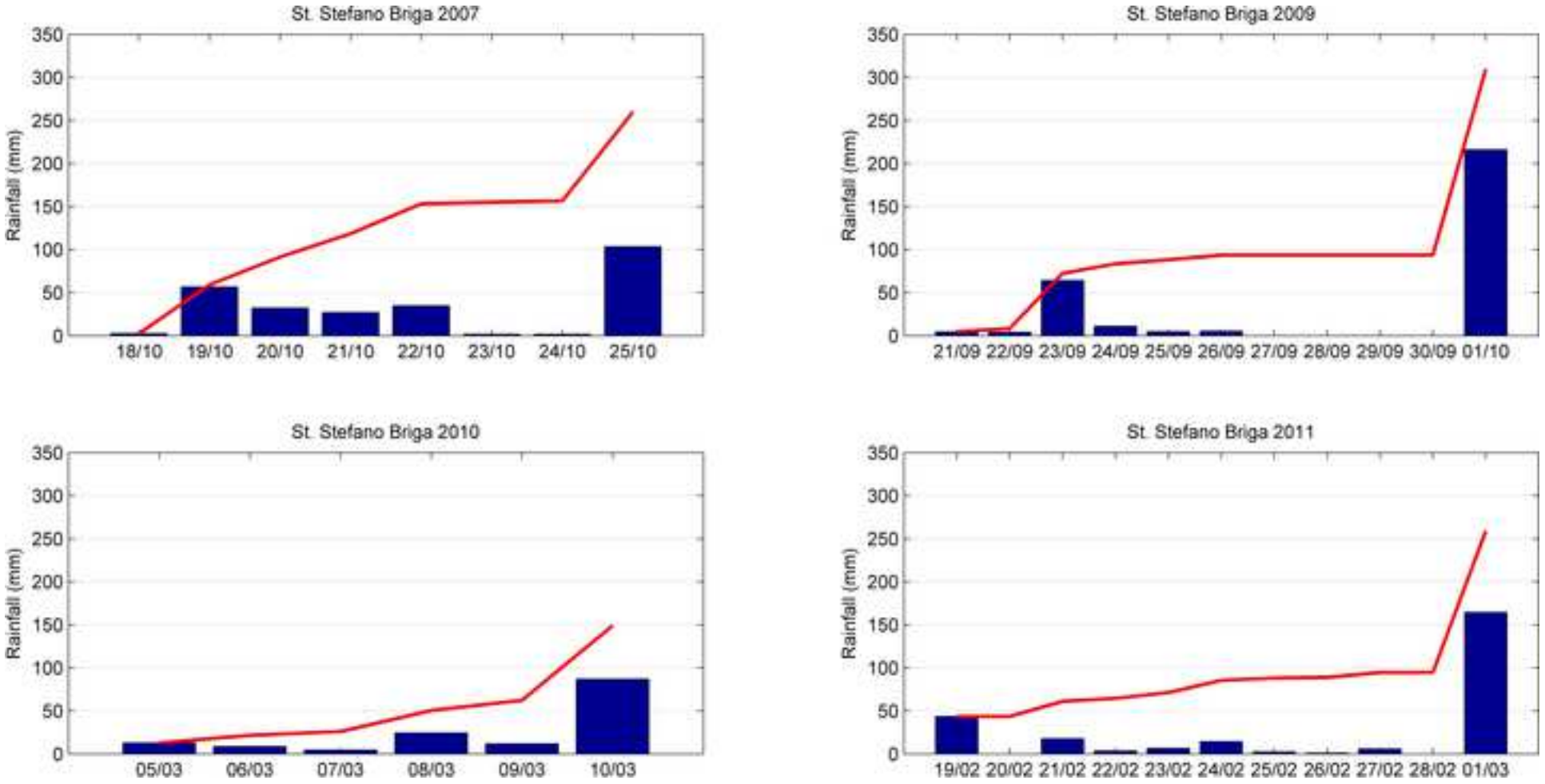

Fig.4

Click here to download Figure fig4.tif

Fig.5

Click here to download Figure fig5.tif

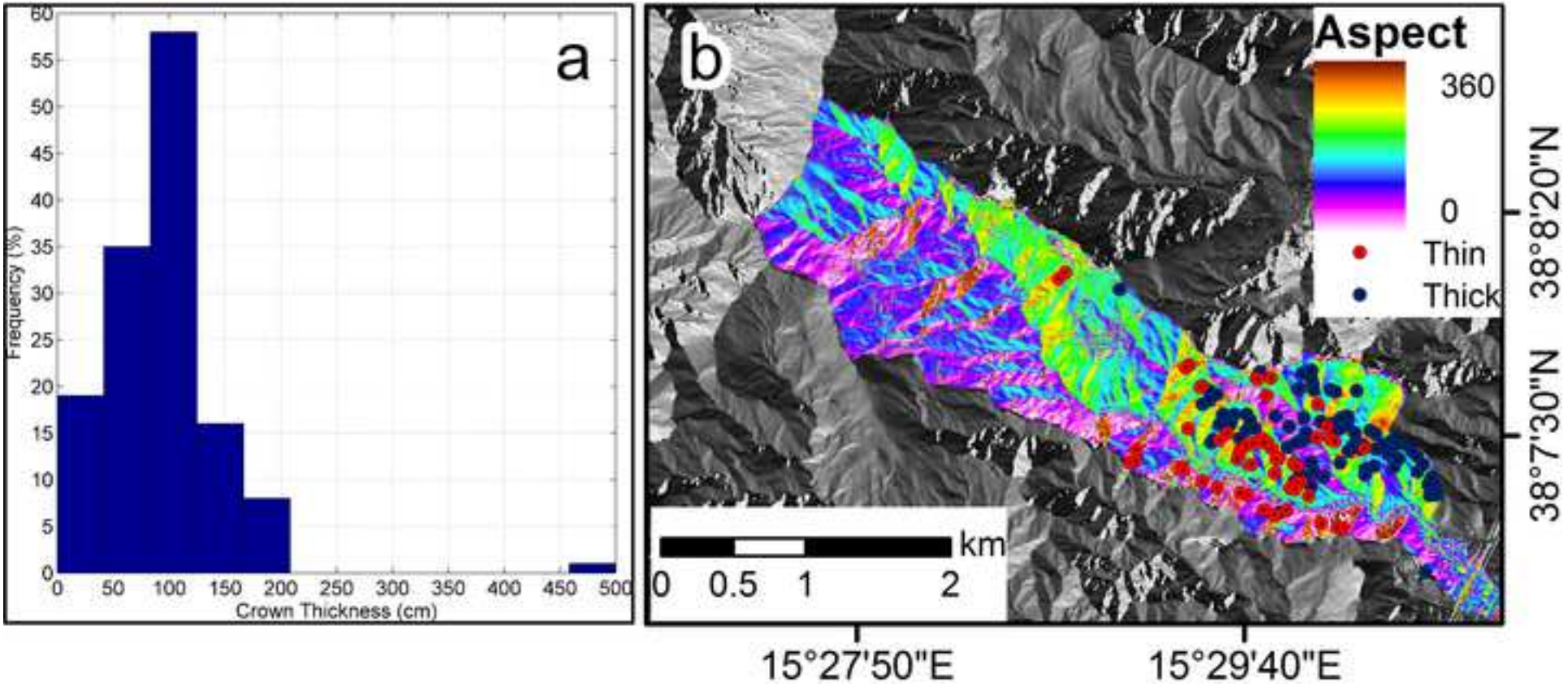

Fig.6

Click here to download Figure fig6.tif

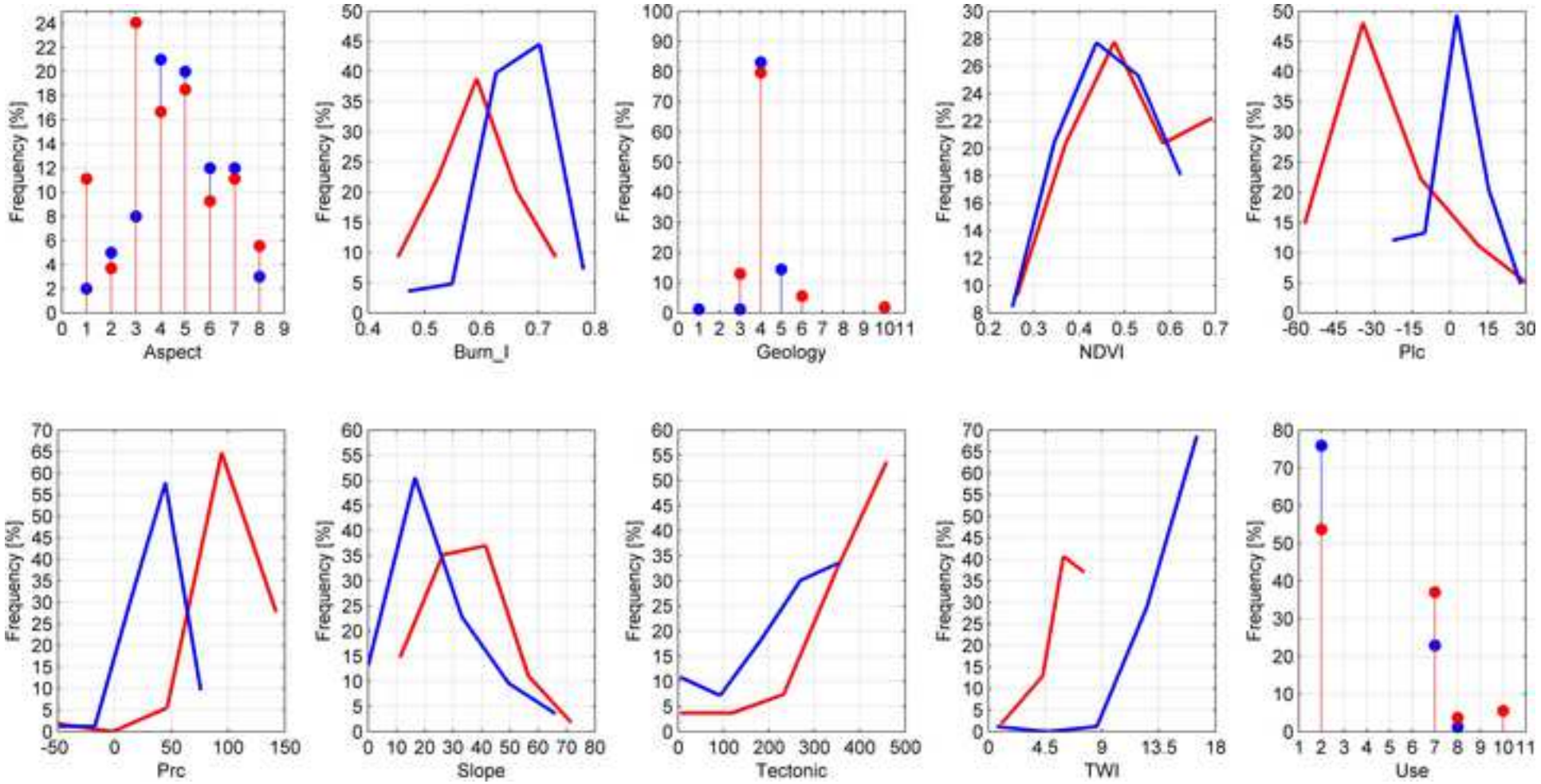

Fig.7

Click here to download Figure fig7.tif

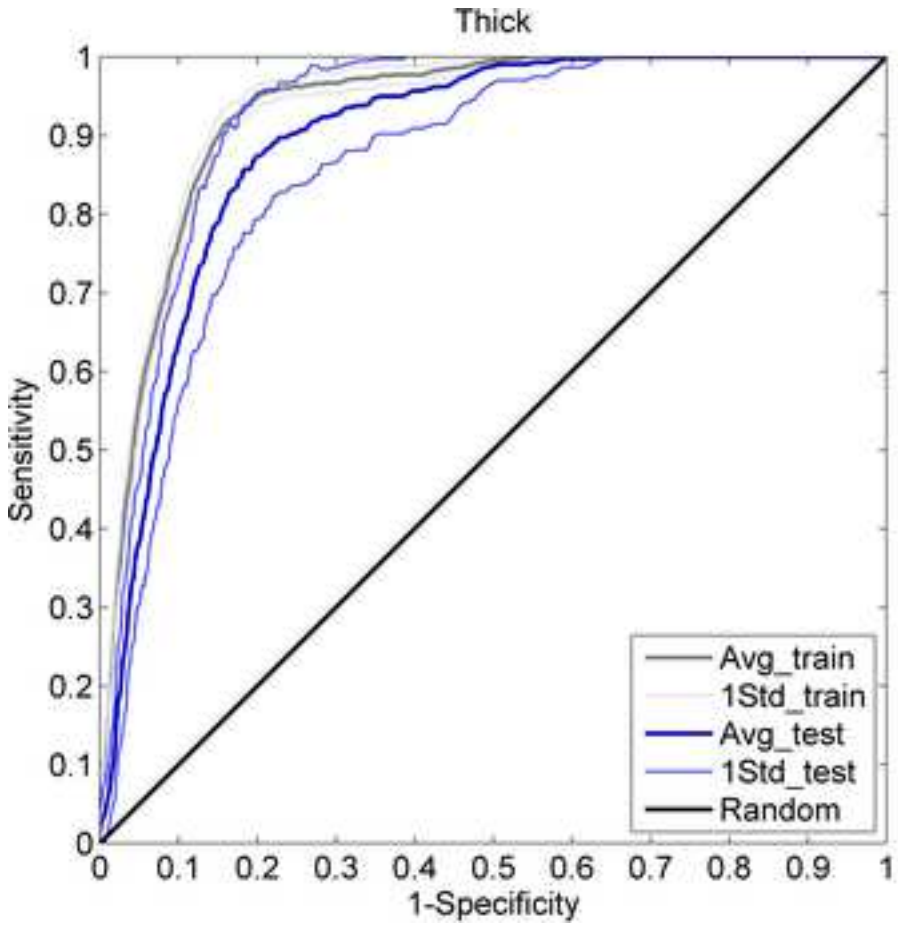

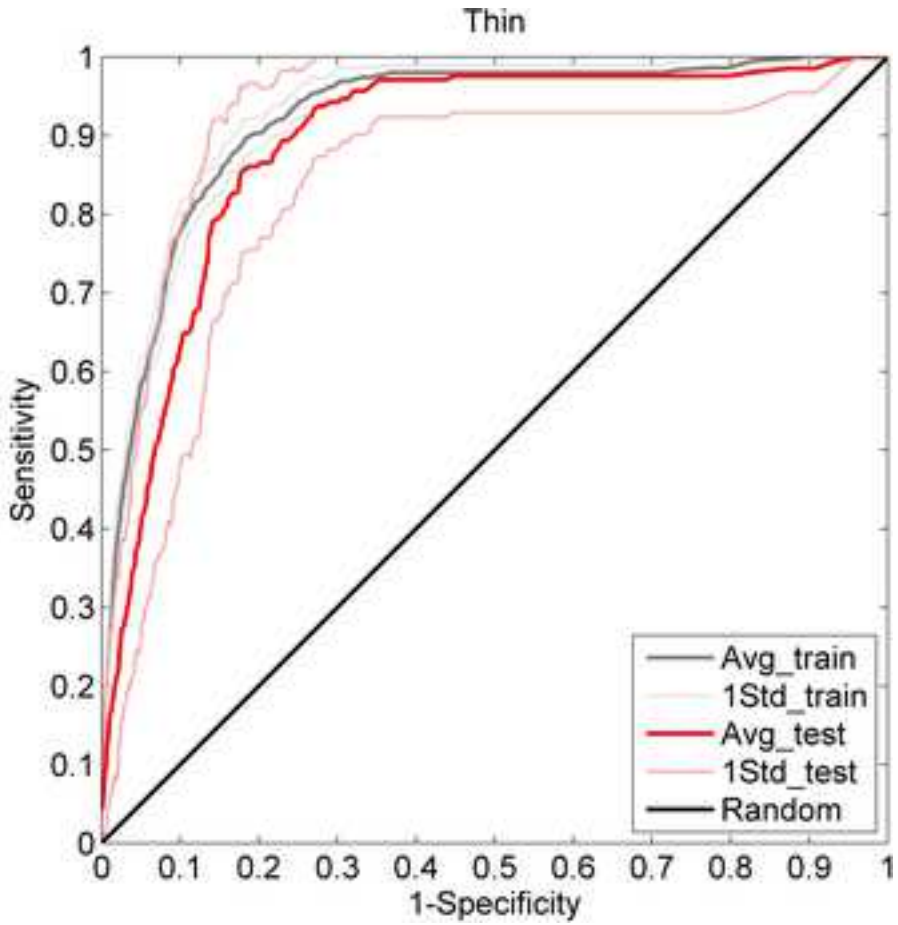

Fig.8

Click here to download Figure fig8.tif

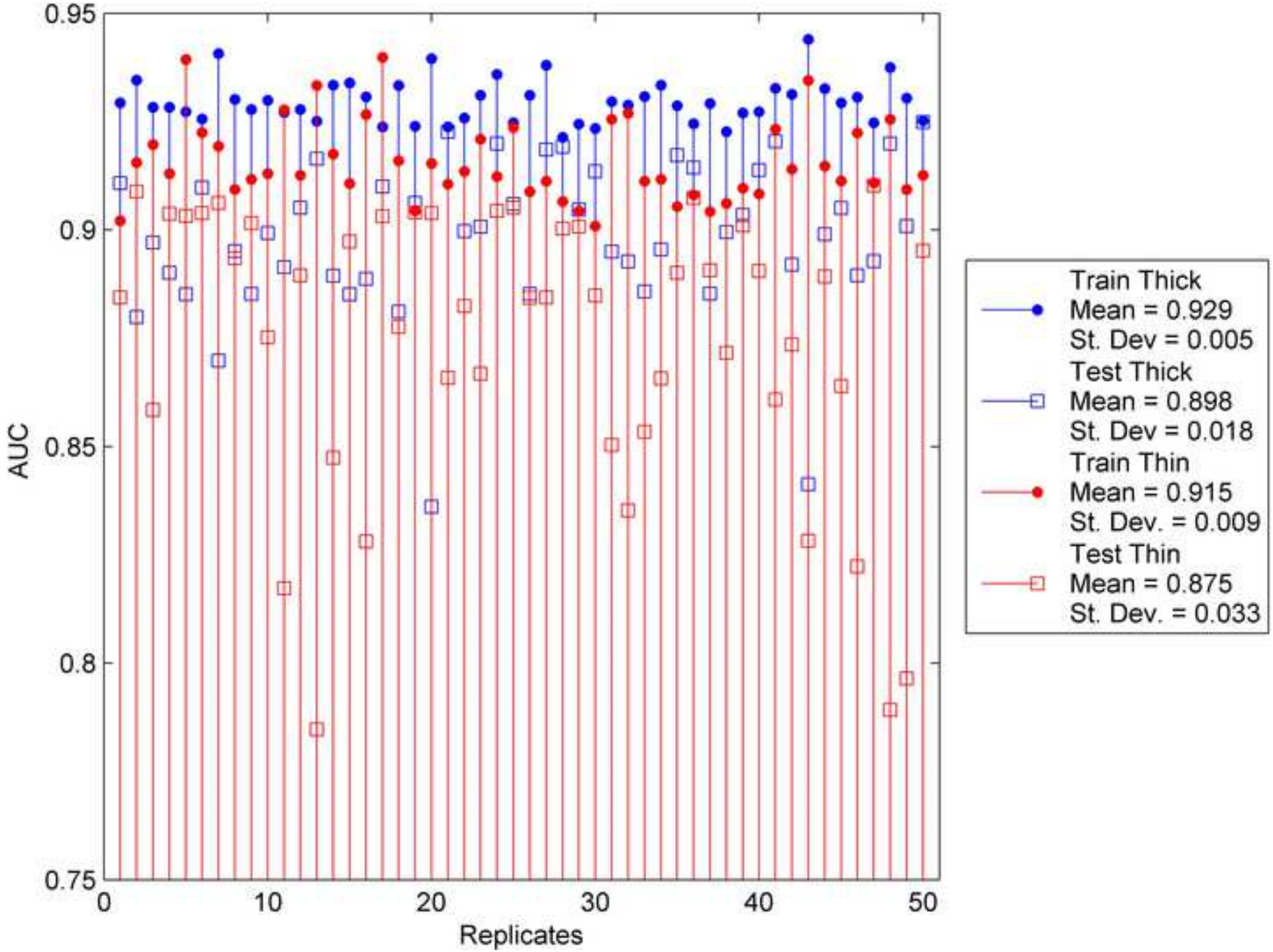

Fig.9

Click here to download Figure fig9.tif

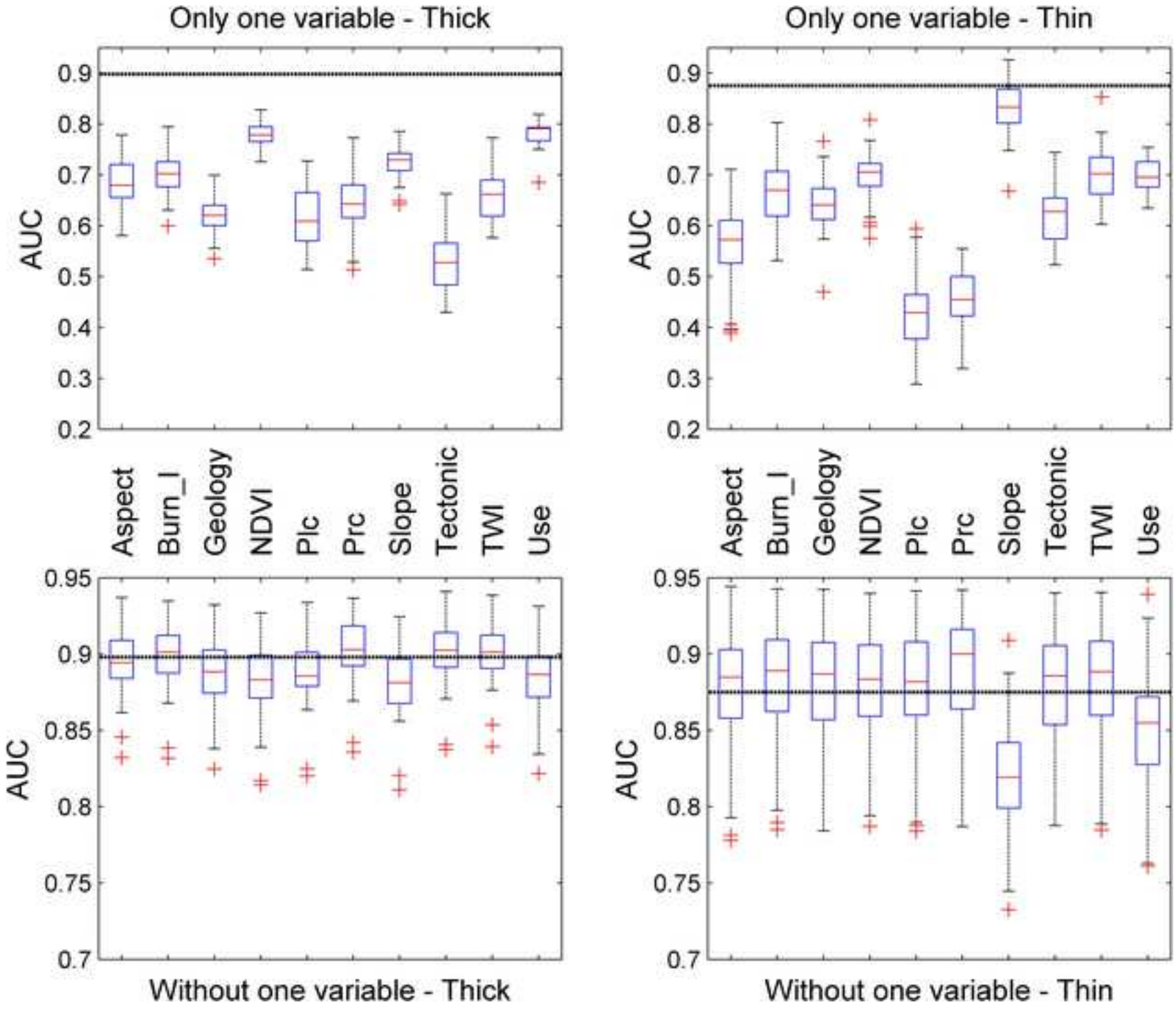

Fig.10

Click here to download Figure fig10.tif

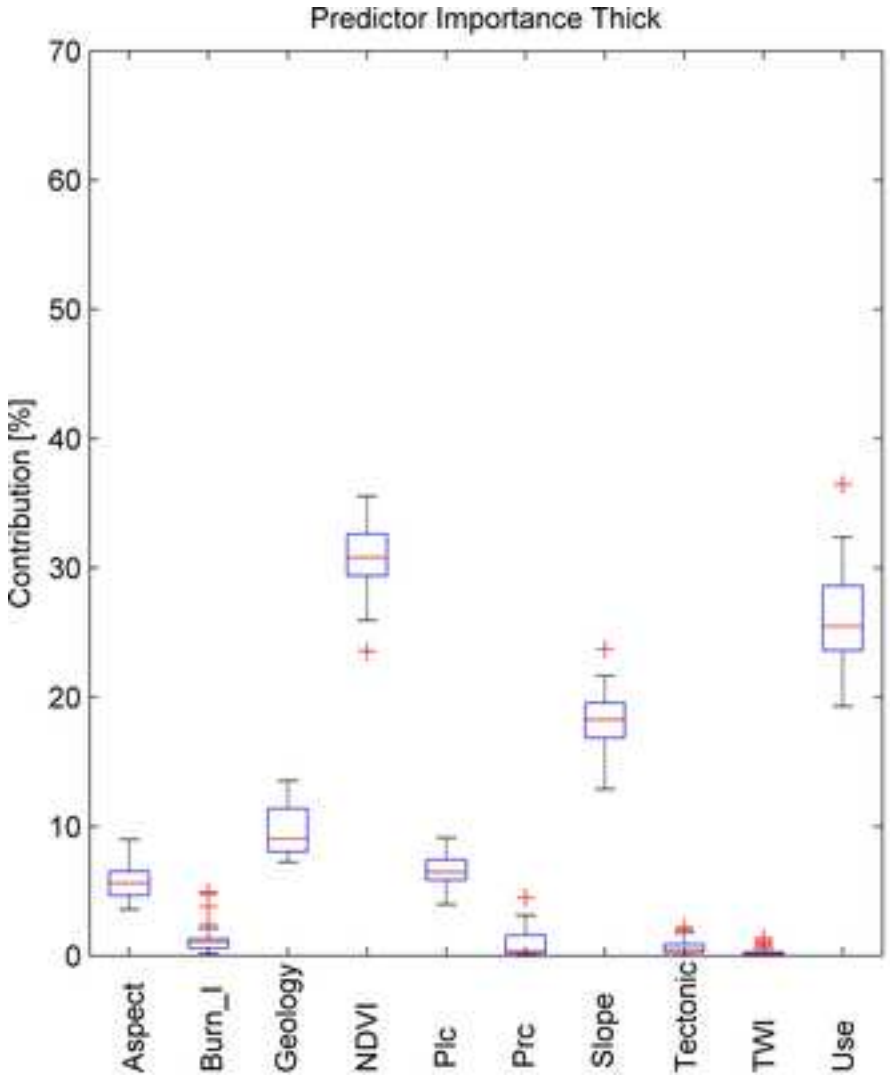

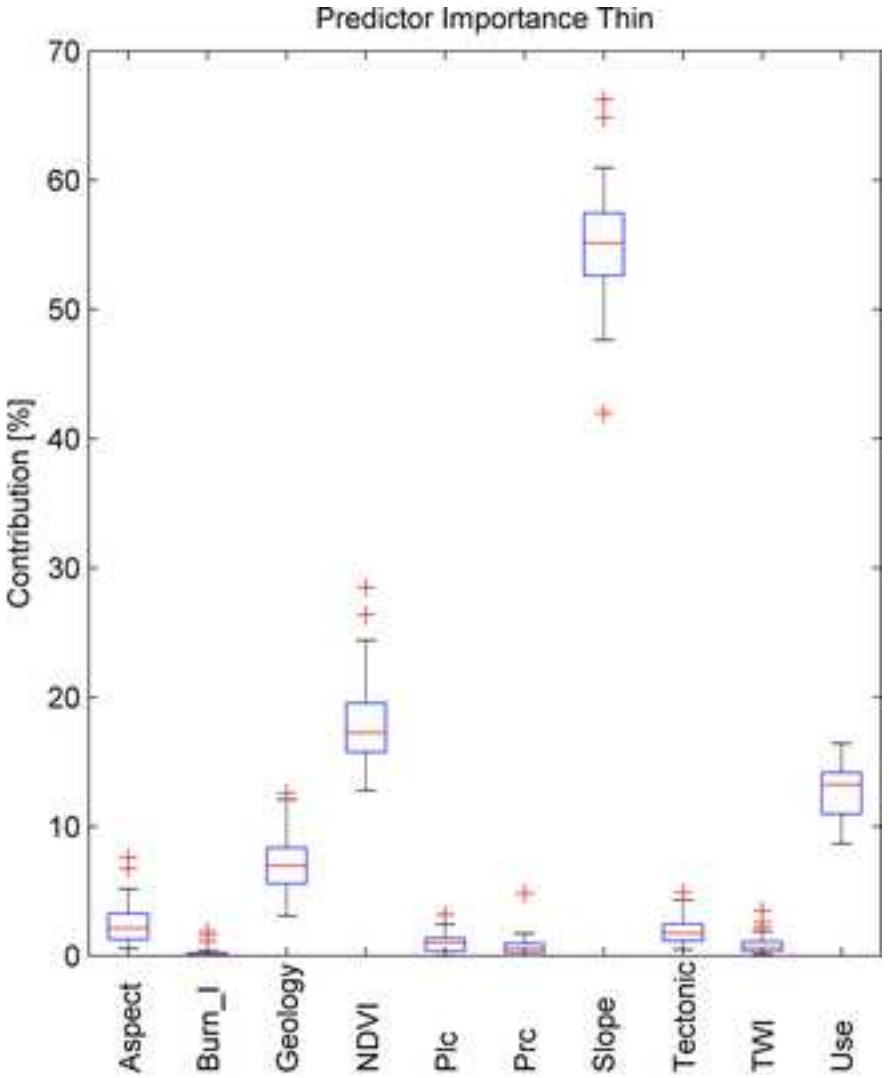

Fig.11

Click here to download Figure fig11.tif

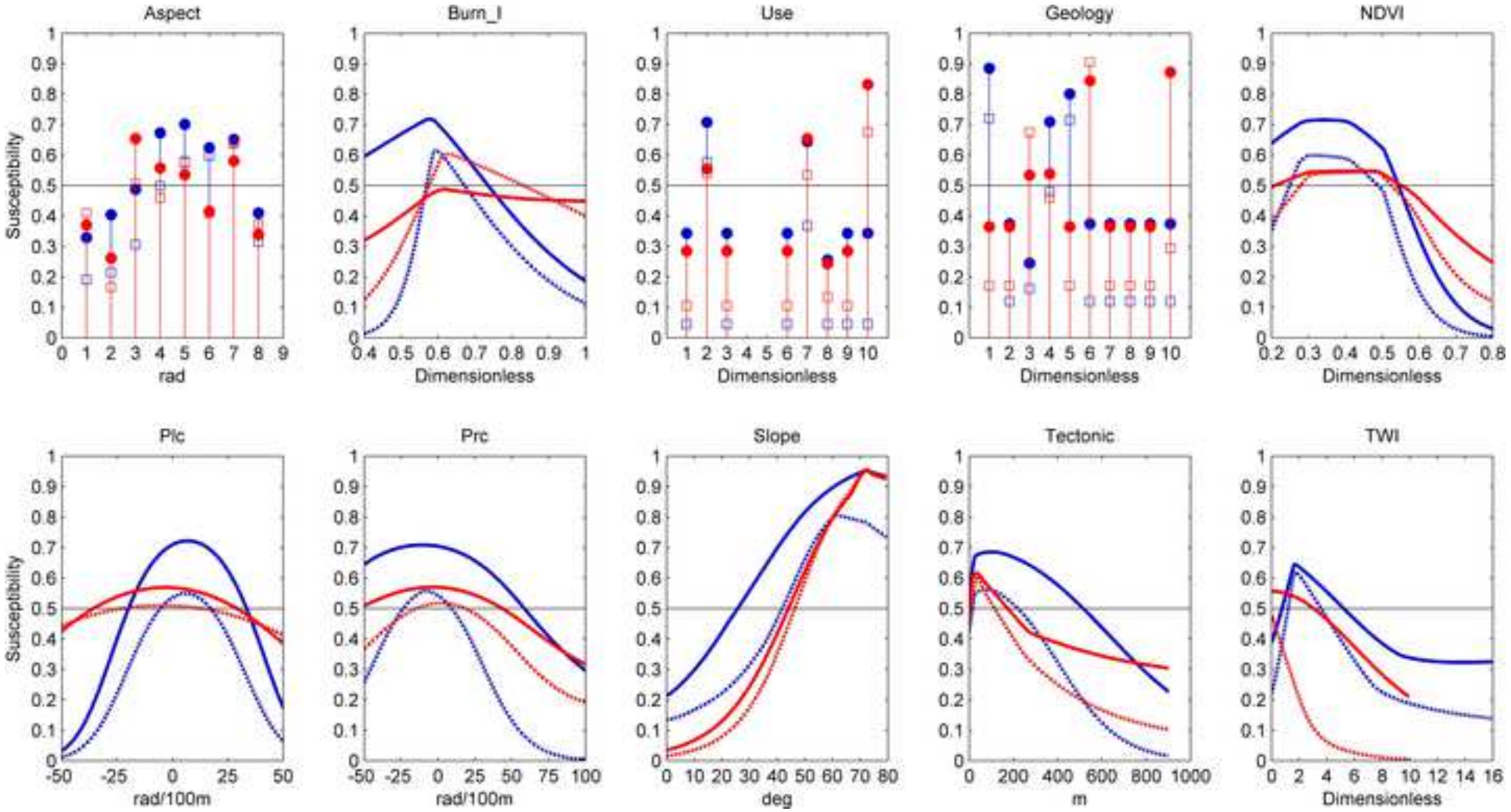

Fig.12

Click here to download Figure fig12.tif

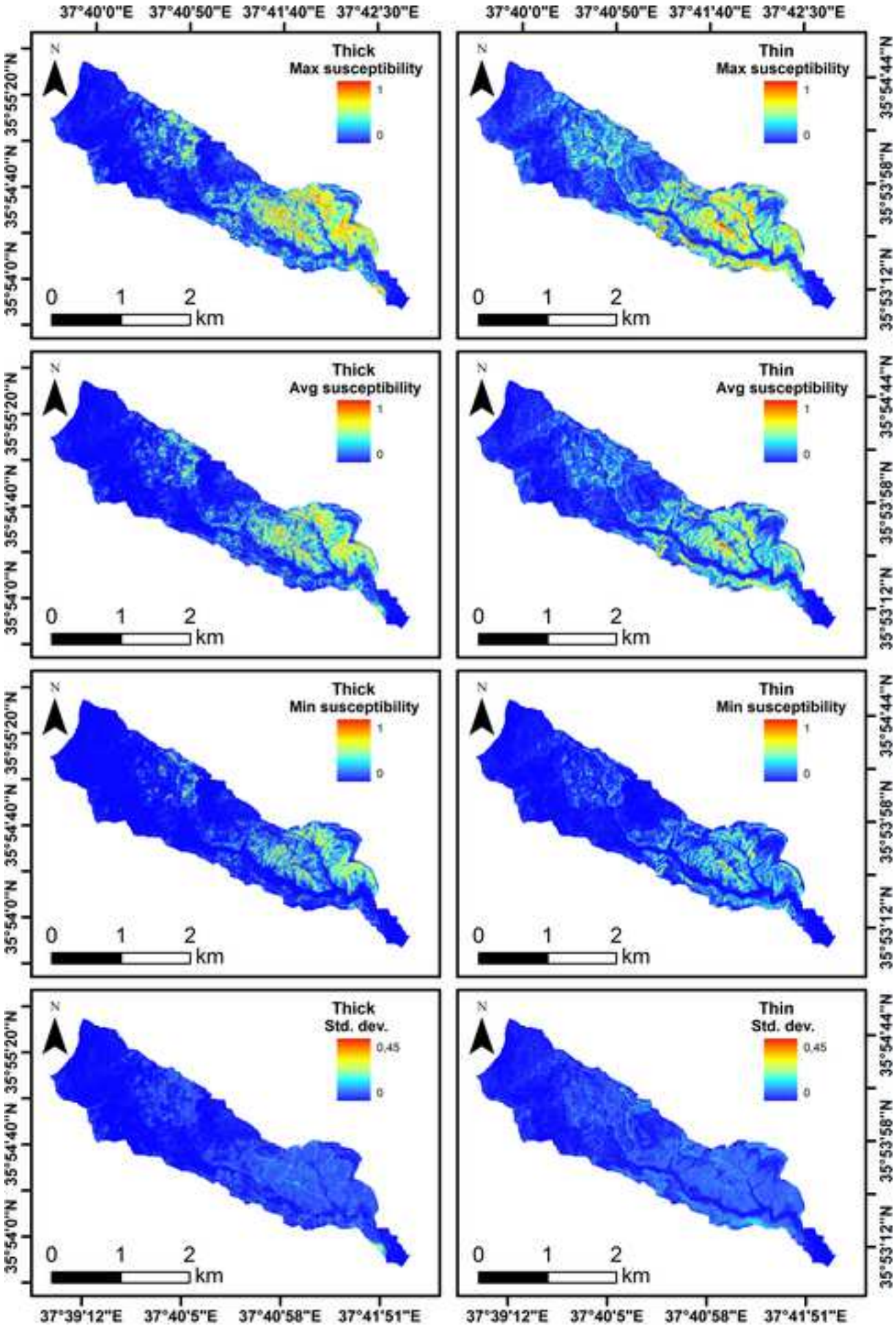

Fig.13

Click here to download Figure fig13.tif

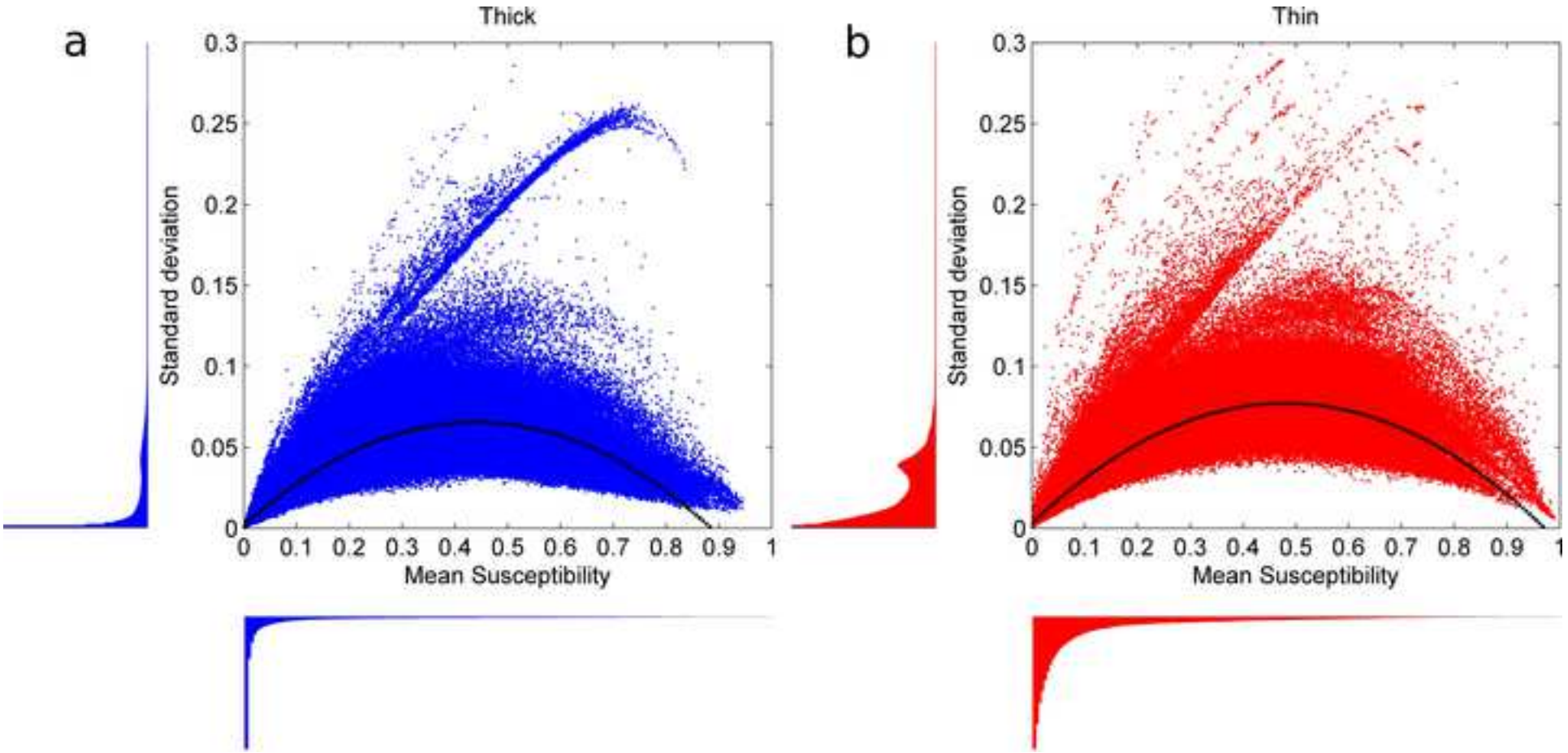

Fig.14

Click here to download Figure fig14.tif